IEEE Access
Multidisciplinary ⋮ Rapid Review ⋮ Open Access Journal

Received 16 April 2023, accepted 9 May 2023, date of publication 18 May 2023, date of current version 30 May 2023.

Digital Object Identifier 10.1109/ACCESS.2023.3277731

RESEARCH ARTICLE

Efficient Estimation of Time-Dependent Brain Functional Connectivity Using Anatomical Connectivity Constraints

HERNAN HERNANDEZ LARZABAL[1,2], DAVID ARAYA[3,4], LAZARA LISET GONZALEZ RODRIGUEZ[1], CLAUDIO ROMAN[1], NELSON TRUJILLO-BARRETO[5], PAMELA GUEVARA[1], (Senior Member, IEEE), AND WAEL EL-DEREDY[4,6,7]

[1]Departamento de Ingeniería Eléctrica, Facultad de Ingeniería, Universidad de Concepción, Concepción 4070386, Chile
[2]Latin American Brain Health Institute (BrainLat), Universidad Adolfo Ibañez, Santiago 7941169, Chile
[3]Facultad de Ingeniería, Universidad Andrés Bello, Santiago 2531015, Chile
[4]Centro de Investigación y Desarrollo en Ingeniería en Salud, Universidad de Valparaíso, Valparaíso 2360102, Chile
[5]Manchester Academic Health Science Centre, Faculty of Biology, Medicine and Health, School of Health Sciences, The University of Manchester, M13 9PL Manchester, U.K.
[6]Department of Electronic Engineering, School of Engineering, Universitat de València, 46003 Valencia, Spain
[7]ValgrAI: Valencian Graduate School and Research Network of Artificial Intelligence, 46022 Valencia, Spain

Corresponding author: Wael El-Deredy (Wael.El-Deredy@uv.cl)

This work was supported in part by Agencia Nacional de Investigación y Desarrollo de Chile (ANID), Chile, under Doctorado Nacional/2017-21170326, under Doctorado Nacional/2017- 21170611, under Doctorado Nacional/2019-21191506, under Fondo Nacional de Desarrollo Científico y Tecnológico (FONDECYT) 1201822, under FONDECYT 1221665, under PIA/Anillo de Investigación en Ciencia y Tecnología (ANILLO) ACT210053 and Financiamiento Basal ANID (BASAL) Centers (FB210008, FB210017, and FB0008); in part by ValgrAI and the Generalitat Valenciana, Spain.

ABSTRACT There is ongoing interest in the dynamics of resting state brain networks (RSNs) as potential predictors of cognitive and behavioural states. Multivariate Autoregressors (MAR) are used to model regional brain activity as a linear combination of past activity in other regions. The coefficients of the MAR are taken as estimates of effective brain connectivity. However, assumption of stationarity, and the large number of coefficients renders the MAR impractical for estimating brain networks from standard neuroimaging time-series of limited durations. We propose HsMM-MAR-AC, a novel sparse hybrid discrete-continuous model for the efficient estimation of time-dependent effective brain networks from non-stationary brain activity time-series. Discrete quasi-stationary Brain States, and the fast switching between them, are modelled by a Hidden semi-Markov Model whose continuous emissions are drawn from a sparse MAR. The coefficients of the MAR are restricted by Anatomical Brain Connectivity information in two ways: 1) Effective direct connectivity between two brain regions is only considered if the corresponding anatomical connection exists; and 2) the autoregressors lag associated with each connection is based on the fiber length between the two regions, such that only one lag per connection is estimated. We test the accuracy of HsMM-MAR-AC in recovering simulated resting state networks of various durations, and at different thresholds of anatomical restrictions. We demonstrate that HsMM-MAR-AC recovers the RSNs more accurately than the benchmark method of the sliding window, with as little as 4 minutes of data. We also show that when the anatomical restrictions are relaxed, longer time-series are needed to estimate the networks, and became computationally unfeasible without anatomical restrictions. HsMM-MAR-AC offers an efficient model for estimating time-dependent Effective Connectivity from neuroimaging data that exploits the advantages of Hidden Markov and MAR models without identifiability problems, excessive demand on data collection, or unnecessary computational effort.

INDEX TERMS Anatomical constraint, brain state, hidden semi Markov model, multivariate autoregressive model, state duration.

The associate editor coordinating the review of this manuscript and approving it for publication was Gustavo Olague.

I. INTRODUCTION

A current challenge in systems neuroscience is to consider the brain as a dynamical system evolving over time. This

involves using neuroimaging data to detect quasi-stable Brain States, and the transitions between them [1], [2], [3], [4], [5], [6]. A Brain State (BS) corresponds to an operational mode with a quasi-stationary activity pattern at the topography, sources, or networks level. This paper focuses on the latter. Recently, the dynamics of brain networks activity in the absence of a cognitive task, the Resting State Networks (RSNs), and the navigation between them over time have attracted the attention as potentially supporting brain function and enabling cognition [7], and marking difference between health and disease [8], [9], [10], [11], [12]. RSNs represent simultaneous, synchronous or coherent activity across multiple brain regions, the configurations of which closely corresponds to the patterns of activity observed during sensory, motor, and cognitive tasks. A number of RSNs has been identified: Default Mode Network (DMN) [13], [14], Sensori-motor Network (SMN) [13], Executive Control Network (ECN) [15], Visual Network (VN) [13], [16], Fronto-Parietal Network (FPN) [13], Auditive Network (AN) [17] and Temporo-Parietal Network (TPN) [17].

Differences in the time-varying occupancy of or switching between RSNs are associated with cognitive and behavioural performance, as well as with psychiatric and neurological conditions [18]. Dynamic functional connectivity captures task-based phenotypes, furthermore relevant functional connectivity behavior emerges from the interconnection of all RSNs [19]. The work of [20] suggests that functional connectivity contains markers that are differentially expressed over time with simultaneous consideration of spatial and temporal characteristics.

Several methods have been proposed to address the RSN detection problem, which can be classified into descriptive and explanatory methods. The former uses features of the measured signals to classify (allocate) time points into specific brain states. The second one can generate or simulate the observed brain signals and their statistical properties (e.g., non-stationary). The descriptive methods use time sliding windows [21], [22], adaptive segmentation by grouping [4], [21], [23], among others [5], [24]. These methods present several problems, such as sensitivity to time window parameter definition, instability of the estimation of the features of interest (e.g., signals' covariance matrix), among others; for more details, see [2] and [3]. The explanatory methods use generative models for characterizing the observed signals [1]. HMM uses a Markov chain to model the transitions between a finite set of hidden discrete RSNs, such that when an RSN is active, it emits an observation. Although HMM addresses many of the shortcomings of descriptive approaches, it has important limitations as a generative model of brain activity. In [2], it was proposed to use HsMM to resolve this limitation. HsMM is a generalization of HMM where the Markov assumption leading to the geometric duration constraint is relaxed to allow the explicit modeling of the RSN duration distribution. The advantages of HsMM over HMM for the modeling of EEG amplitude fluctuations (signal envelope data) are demonstrated in [2]. This paper proposes an efficient method of using neuroimaging data to recover RSNs characterized by transiently stationary large-scale causal interactions (directed information flow) between different brain regions, henceforth time-dependent Effective Connectivity (tdEC).

In the context of network-level analysis, previous work has capitalized on the flexibility and simplicity of Multivariate Autoregressive (MAR) models for modeling causal brain networks. In a MAR, the output signals represent the temporal evolution of the activity of a node (a brain area) of the brain network; and they are modeled as a linear combination of the past activity of the other nodes. Therefore the coefficients of the linear combination (MAR coefficients) provide a characterization of the causal interactions (directed information flow) between different nodes of the brain network [1], [3], [25], [26], [27]. The work of [1] is one of the first models that used switching MARs to model a time-dependent causal network, implemented a RSN allocation method using a Bayesian generative model where brain signals were temporally clustered (segmented) into time periods (i.e., RSN) characterized by stationary MAR models. Therefore [1] proposes adding a level of flexibility using temporal clusters characterized by MAR models. However, it is impossible to provide a transition probability between mesostates with this approach. The research of [28] proposes HMM to model the RSN transitions. This approach, however, inherits the shortcomings intrinsic to HMM. Furthermore, the identification of a MAR with unknown number of lags, for large-scale brain networks in the source domain quickly becomes intractable. For example, if we consider that the brain consists of 62 areas (based on Desikan Killiany parcelation [29]), and we use a MAR order of 10 and 10 brain states, a total of 384 400 parameters have to be estimated ($62 \times 62 \times 10 \times 10$). Each coefficient is modeled as a mean and covariance matrix, so the number of parameters to be estimated is much more. Such a complex model can lead to overfitting or identifiability issues if enough data is unavailable [30], [31]. This problem can be addressed in different ways. In [3], the authors introduced a parameterization of the MAR matrix of coefficients, reducing the number of parameters to be estimated. This parameterization, although mathematically convenient, might impose physiological unrealistic constraints on the model. Another option is to increase the available data to fit the model by concatenating several subjects' data along the time dimension [28]. However, this approach is only valid if RSN features can be assumed to be invariant across subjects. An alternative option is to pre-select a limited set of brain areas in advance to reduce the dimensionality of the MAR. The risk of this solution is the appearance of erroneous connections due to the interference of areas that are not included in the study [32], [33].

Here we propose to drastically reduce the number of MAR coefficients by using the sparseness of the anatomical connectivity information. Since functional integration between

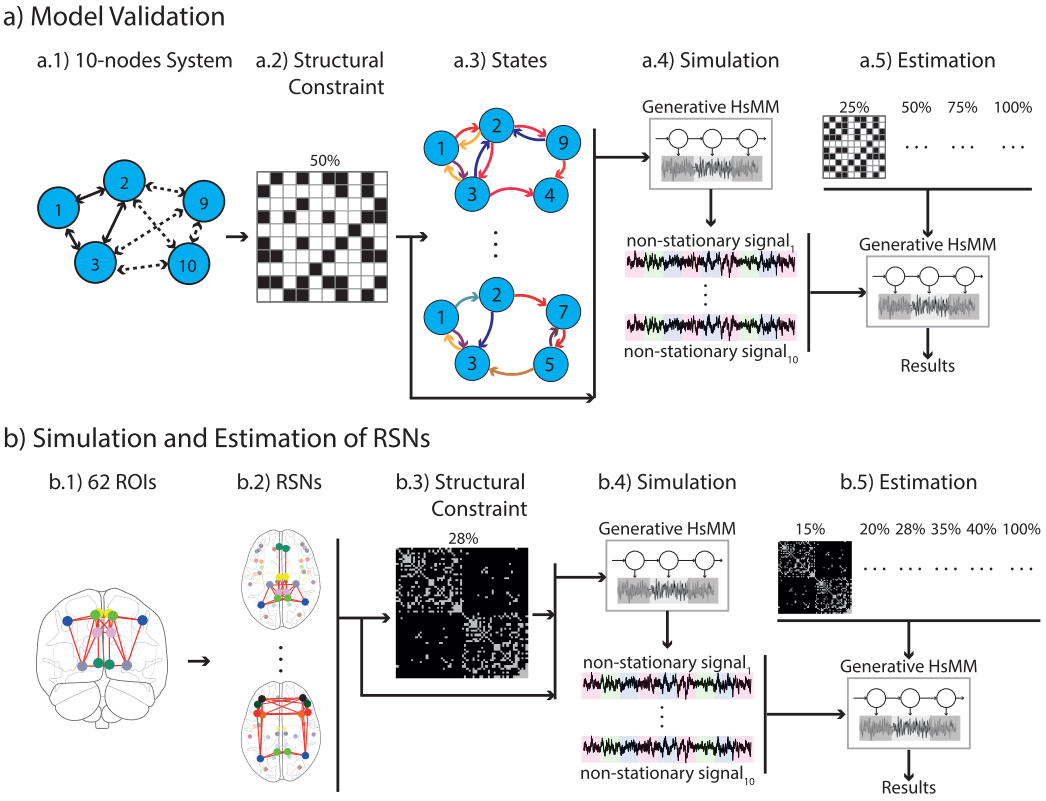

FIGURE 1. **Pipeline of the presented experiments. (a) Experiment 1 is an essential validation of the proposed HsMM-MAR-AC on a toy system of 10 nodes (a.1), whose structural connectivity is assigned randomly, and thresholded to allow 50% of the connections, to define the anatomical constraints (a.2). Systems with 3, 4, and 5 states (network configurations) were defined (a.3). Ten non-stationary node signals were simulated from the generative HsMM-MAR-AC model as described in section II-A. (a.4). The coefficients are estimated at varying levels of anatomical constraints (a.5) as explained in methods section II-C1. (b) Experiment 2: Stimulation and estimation of brain RSNs. b.1) A 62-node system was designed based on the DKT atlas. (b.2) The system contained 7 states based on the 7 most reported RSNs, section II-B3 for details. (b.3) The AC was calculated by applying a threshold to the connection weights (section II-B4), allowing all nodes of the 7 RSNs to be connected to at least one other node, section II-B1. (b.4) Ten non-stationary signals were simulated from the generative model HsMM- MAR-AC. (b.5) The estimation step was performed by varying the AC and the duration of the signal, as explained in methods section II-C2.**

different brain areas is mediated by white matter (WM) connections [34], it follows that MAR coefficients should only be estimated where the effective connection is supported by anatomical connectivity. Furthermore, the length of the fiber between two connected regions determines the time delay of the signal between them, [35], [36], and [37], such that only one MAR coefficient per connection can be estimated. Several studies have reported that functional dynamics reflects anatomical connectivity [38], [39], [40], such that the time-dependant effective connectivity fluctuates around an anatomical connectome [41], [42], [43]. These findings suggest that anatomical connectivity could be used as a constraint for estimating functional or effective connectivity. Such constraint has previously been suggested to limit the complexity of the MAR and to estimate static functional connectivity [35], [44], [45].

In this paper we implemented an HsMM with MAR emissions, whose sparse coefficients are constrained by anatomical connectivity, hence HsMM-MAR-AC. We evaluate the benefit of using anatomical connectivity constraints in estimating the tdEC of the RSNs and their temporal dynamics, compared to the moving window benchmark. Although anatomical information in this work was derived from the human connectome, the proposed approach could also be used to incorporate individual anatomical information should such data be available. In studies such as [35], [44], and [45], anatomical connectivity is applied as a constraint to MAR models of high complexity. However, these studies do not consider the dynamics of brain states. In addition, an arbitrary threshold is applied to define the Anatomical Constraint (AC), as in [35], we modified it to detect the strongest connections of the RSNs.

The paper is organized as follows. Section II-A presents the theoretical basis of HsMM-MAR-AC model, and the estimation of the model parameters. Section II-B presents the calculation of the anatomical connectivity information and the constraint. Section II-C describes the generation

of the validation data, and the validation experiments. Section II-D contains the metrics to evaluate the performance of the proposed model. Section II-E presents the methods for RSN estimation that we compare with HsMM-MAR-AC. Subsequently, in Section III, we show a detailed evaluation of the method based on two simulated experiments. The first experiment is carried out to validate the performance of the algorithm in two key aspects: a) the verification of the parameter recovery of the original model and b) the evaluation of the prediction capacity of the model in new data. The second experiment is performed to validate the model's ability to recover RSNs and their dynamics. The third experiment focuses on using the most commonly used algorithms in the literature to compare our algorithm's performance. Finally, Section IV presents an analysis of the proposed model's results and scope.

II. METHODS

We describe an HsMM-MAR-AC model for RSN allocation, where RSN is defined as a specific configuration of an effective brain network that persists over short periods of time, generating a continuous sequence of the observed brain activity before switching to another RSN. Next, We elucidate how the anatomical connectome information can reduce the model's description and hence the number of parameters to be estimated. Finally, We describe the inversion procedure to estimate the parameters using the Bayesian machinery and the performance metrics and experiments used to evaluate the accuracy and efficiency of the model. Figure 1 shows the general pipeline used in this work. We divide the work into two experiments; the first aims to validate the performance of the algorithm (see Section II-C1), and the second measures the ability of the algorithm to detect RSNs (see Section II-C2).

A. THE GENERATIVE MODEL

1) MAR MODEL DESCRIPTION

This model characterizes the neuronal activity of each area as a node of the network. The activity of node X corresponds to the linear combination of the activity in the past (with delay) of the other areas connected to X. The interaction between the nodes is not instantaneous; each interaction will take place in a specific delay (from 1 to L). Furthermore, each interaction towards X must be modulated by an Autoregressive coefficient. Finally, Gaussian noise is incorporated into the resulting neuronal activity. As an illustrative example, we consider a simple arbitrary system comprising three nodes that are connected to a node n. This can be represented as follows:

$$y_{nt} = \beta_1 \times y_{1(t-5)} + \beta_2 \times y_{2(t-6)} + \beta_3 \times y_{3(t-7)} + e_t \quad (1)$$

where y_{nt} corresponds to the neuronal activity of the nodes n at time t, β_n denotes the autoregressive coefficient, and e_t is the noise Gaussian. In this case, there is a neural connection from nodes 1, 2, and 3 to node n, which implies that the neuronal activity of node n is determined by the linear combination of the activity of nodes 1, 2, and 3 at delays 5, 6, and 7 respectively.

2) HsMM-MAR-AC MODEL DESCRIPTION

The model comprises two components: The HsMM characterizes the time-dependent brain effective connectivity as rapid transitions between discrete RSNs that persist over a short duration in time [2]. For each state, the brain activity in each brain area is defined by the activity and effective (time-lagged) connections among brain areas, described by the second component, the MAR, forming a stationary (or quasi-stationary) network [1], [28], [46]. Figure 2 shows the dynamic Bayesian network (DBN) graph representation of the model with the conditional dependencies between the parameters, hidden variables, and the observed data.

Where:

- N Number of nodes,
- M Number of states,
- L Maximum delay,
- y_t Observed current density (brain activity) at time t in each brain area,
- s_t Hidden RSN at time t. Here there are M states,
- τ_t Remaining time in the RSN s_t,
- W Set of matrices of MAR coefficients, one for each RSN, with $W = \{W^{(1)}, W^{(2)}, \ldots, \ldots, W^{(M)}\}$,
- Λ Set of matrices that contain their corresponding precisions, with $\Lambda = \{\Lambda^{(1)}, \Lambda^{(2)}, \ldots, \ldots, \Lambda^{(M)}\}$,
- Φ Set of vectors of observation noise precision, with $\Phi = \{\phi^{(1)}, \phi^{(2)}, \ldots, \ldots, \phi^{(M)}\}$,
- A Matrix of transition probabilities ($M \times M$) between RSNs,
- U Set of M values that denote the mean duration of each RSN, with $U = \{\mu^{(1)}, \mu^{(2)}, \ldots, \ldots, \mu^{(M)}\}$,
- Z Set of M values that denote their corresponding precisions, with $Z = \{\zeta^{(1)}, \zeta^{(2)}, \ldots, \ldots, \zeta^{(M)}\}$.

The full likelihood function of Figure 2 is expressed as:

$$\begin{aligned} &P(y_{1:T}, s_{1:T}, \tau_{1:T}, \Phi, W, \Lambda, A, U, Z) \\ &= P(s_1, \tau_1) \times \prod_{t=2}^{T} P(s_t, \tau_t | s_{t-1}, \tau_{t-1}, A, U, Z) \\ &\quad \times P(y_t | W, \Phi, s_t, \tau_t) \times P(\Phi) \times P(A) \\ &\quad \times P(W|\Lambda) \times P(\Lambda) \times P(U) \times P(Z) \end{aligned} \quad (2)$$

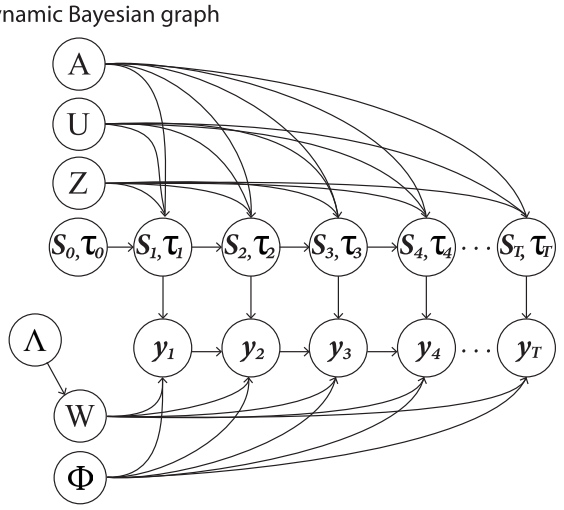

FIGURE 2. Dynamic Bayesian graph of the generative probabilistic HsMM-MAR model. If the model is in state s_T, it emits a sequence of measurable brain activity y_T according to the rules specified by the MAR coefficients in $W^{(M)}$, for a duration given by $U = \mu^{(M)}$ and $Z = \zeta^{(M)}$. When s_t runs out of time τ_t, the model switches probabilistically to another RSN according to the transition matrix A.

The probability of emitting an observation y_t at instant t given that the state s_t of duration τ_t corresponds to:

$$\begin{aligned}&\log\left(P(y_t|W,\Phi,s_t,\tau_t)\right)\\&=\sum_{k=1}^{M}\sum_{d=1}^{D}\delta\big((s_t,\tau_t),(k,d)\big)\\&\quad\times\log\left(N(y_t|W^{(k)}\times x_{\cdot t},Diag(\phi^{(k)})^{-1})\right)\end{aligned}\tag{3}$$

where $x_{\cdot t} = (y_{\cdot(t-1)}{}^T, y_{\cdot(t-2)}{}^T, \ldots y_{\cdot(t-l)}{}^T)$ denotes the t column of the matrix X corresponding the to past observations in each brain area, i.e., the regressors. The autoregressive coefficients to estimate in Equation (3) are the elements of matrix W, which corresponds to a full matrix of dimensions $N \times (N \times L)$. The n row of the matrix W corresponds to the autoregressive coefficients associated with the n input of y_t.

For instance, considering a brain defined by the DKT atlas [29], which contains 62 areas, a maximum lag of 10, and 7 brain states, then the number of autoregressive coefficients to estimate is $62 \times 62 \times 10 \times 7 = 269\,080$.

Here we use anatomical connectivity information to reduce this number in two ways: limiting the connectivity matrix to only where anatomical connectivity exists (see Section II-C1) and using the tractography data to calculate the precise fiber length and thus estimate the delay between two regions (see Section II-C2). The delay restricts the number of connection between regions to just one. In the above example, if half the connections were considered and one lag is estimated, then the number of coefficients drops to $1/2 \times 62 \times 62 \times 1 \times 7 = 13\,454$, which is approximately 6% of the original number of coefficients.

The multivariate Gaussian probability density of the N areas in Equation (3) is separated into N uni-variable Gaussian distributions to implement this reduction. This is feasible since the precision matrix $Diag(\phi^{(k)})$ has only elements on the diagonal (they are considered independent). Regarding the source n, we have that the new precision is $\phi_n^{(k)}$ and corresponds to element n of the diagonal of the matrix $Diag(\phi^{(k)})$.

In addition, the Gaussian means described in Equation (3) by $W^{(k)} \times x_{\cdot t}$ is modified by $w_{n\cdot}^{(k)T} \times x_{\cdot t}$, where $w_{n\cdot}^{(k)}$ denotes the vector of column n of the coefficient matrix W. This is where the anatomical information is used, which is translated in having a vector l_n extracted from the connectivity matrix estimated in Section II-B1 that contains the indices of those connections not discarded for source n. That is, those connections are most likely and correspond to the estimated delay. Using this vector, we calculate the mean of the Gaussian of the source n; and we can write it as $w_{n\mathbf{l_n}}^{(k)T} \times x_{\mathbf{l_n}t}$, where these variables correspond to a subset of $w_{n\cdot}^{(k)}$ and $x_{\cdot t}$ respectively, based on the indices of l_n. With this modification, Equation (3) becomes Equation (4).

$$\begin{aligned}&\log\left(P(y_t|W,\Phi,s_t,\tau_t)\right)\\&=\sum_{k=1}^{M}\sum_{d=1}^{D}\sum_{n=1}^{N}\delta\big((s_t,\tau_t),(k,d)\big)\\&\quad\times\log\left(N(y_{nt}|w_{n\mathbf{l_n}}^{(k)T}\times x_{\mathbf{l_n}t},\phi_n^{(k)-1})\right)\end{aligned}\tag{4}$$

3) HsMM-MAR-AC PRIORS

We model the MAR coefficients using a zero mean multivariate Gaussian and precision matrix with only elements on the diagonal, which considers independence among the coefficients (see Equation (5)).

$$\begin{aligned}P(W|\Lambda)&=\prod_{k=1}^{M}P(W^{(k)}|\Lambda^{(k)})\\&=\prod_{k=1}^{M}\prod_{n=1}^{N}N\left(w_{n\mathbf{l_n}}^{(k)}|0,Diag(\lambda_{n\mathbf{l_n}}^{(k)})^{-1}\right)\end{aligned}\tag{5}$$

where $\lambda_{n\mathbf{l_n}}^{(k)}$ represents a subset of $\lambda_{n\cdot}^{(k)}$ according to the index of l_n in state k.

The Gaussian distribution dimension that describes $w_{n\mathbf{l_n}}^{(k)}$ represents the total number of indices contained in l_n.

$$\begin{aligned}P(\Lambda)&=\prod_{k=1}^{M}P(\Lambda^{(k)})\\&=\prod_{k=1}^{M}\prod_{n=1}^{N}\prod_{j\in l_n}Gam(\lambda_{nj}^{(k)}|\hat{b}_{nj},\hat{c}_{nj})\end{aligned}\tag{6}$$

where λ_{nj} represents the j-component of the vector $\lambda_{n\mathbf{l_n}}$. In addition, $\hat{b}_{nj}$ and $\hat{c}_{nj}$ define the shape and scale parameters of the Gamma distribution. We use a non-informative prior with $\hat{b}_{nj} = 1000$ and $\hat{c}_{nj} = 0.001$, based on [47]. We assumed that the noise of the signal was distributed according to a Gaussian distribution with a zero mean and a diagonal

covariance matrix.

$$P(\Phi) = \prod_{k=1}^{M} P(\phi^{(k)}) = \prod_{k=1}^{M}\prod_{n=1}^{N} P(\phi_n^{(k)}) = \prod_{k=1}^{M}\prod_{n=1}^{N} Gam(\phi_n^{(k)}|\hat{e}_n, \hat{f}_n) \quad (7)$$

where $\hat{e}$ and $\hat{f}$ represent the shape and scale parameters of the Gamma distribution. Those values are set to 1 000 and 0.001, respectively.

For the description of the other model parameters (i.e., transition, duration of the states, and initial state), see [2].

4) MODEL PARAMETERS ESTIMATION

No analytical solutions were found in the parameters model estimation. Thus, the estimation of the parameters was performed using an approximate inference method called Variational Bayes (VB) [30], [48]. VB uses an auxiliary function $q(x)$ to approximate the posterior distribution of the parameters and/or hidden variables as closely as possible. The Mean Field Approximation (MFP) approach proposed in [49] allowed for the selection of a factorizable $q(x)$. We use conjugate priors to calculate the analytical expression of updated parameters and hidden variables in time. The MFP used for the joint probability was:

$$\begin{aligned} &q(y_{1:T}, s_{1:T}, \tau_{1:T}, \Gamma, W, \Lambda, A, \mu, \rho) \\ &= q(y_{1:T}) \times q(s_{1:T}, \tau_{1:T}) \times q(\Phi) \times q(W) \\ &\quad \times q(\Lambda) \times q(A) \times q(U) \times q(Z) \end{aligned} \quad (8)$$

For complete details about model parameters and their estimation, see Appendix A.

B. ANATOMICAL CONSTRAINT

1) ANATOMICAL CONNECTOME CALCULATION

Whole-brain probabilistic tractography was reconstructed using the software MRtrix, based on the spherical deconvolution model proposed by [50]. Anatomically-Constrained Tractography (ACT) [51] was calculated with: step size = $0.1 \times voxelsize$, angular threshold= 90°, minimum length = 30 mm, maximum length = 250 mm, cutoffvalue = 0.06, and 30 million streamlines. Each tractography dataset was filtered with SIFT tool (Spherical-deconvolution Informed Filtering of Tractograms) presented in [52], maintaining 3 million of fibers. The tractography was computed using dMRI data from 106 subjects from the HCP database [1] and each subject was normalized to the MNI space [53], using the corresponding non-linear transformation.

Figure 3(a) shows the pipeline used for calculating the average weighted connectivity matrix. We computed the connectivity matrix the probabilistic tractography datasets and the anatomical Desikan Killiany (DKT) atlas [29]. This matrix contains the number of fibers (F_{ij}) connecting ROI$_i$ and ROI$_j$. Figure 3(b) illustrates the approach for calculating the anatomical connectivity. We chose the most repeated ROI evaluating a neighborhood of 5 mm for each fiber extreme point. This approach, combined with ACT, obtains better labeling than when using only the extreme point or all the voxels intersecting the path of the fiber [54]. Hence, we constructed the individual connectivity matrices (62×62) representing the F_{ij} of each pair of anatomical ROIs. We calculated the individual weighted connectivity matrix ($w_{subject_i}$), based on the connection strength (w) between each pair of ROIs (see Equation (9) and [55], [56]), where n_i and n_j are the volume of ROI$_i$ and ROI$_j$, respectively.

$$w_{ij} = \frac{2F_{ij}}{n_i + n_j} \quad (9)$$

The average weighted connectivity matrix w_{mean} was calculated, from the 106 individual weighted connectivity matrices. We used w_{mean} and different thresholds for defining the percentage of connections, which we used to define different ACs, including the reference AC (see Section II-B4).

2) CALCULATION OF THE MAR LAGS

We calculate the conduction delay between two connected regions as the average path length of connecting fibers divided by the conduction velocity for myelinized axons of 6 m/s [57]. Additionally, the conduction velocity for self-connections is set to 3 m/s [35]. The path length of each fiber (L) was calculated by adding the Euclidean distance between consecutive points (see Figure 3(c)). The conduction delay is converted to MAR lag by dividing the delay by the temporal resolution of the data, here 5 ms.

3) RESTING STATE NETWORKS

We employed the seven most reported RSNs. These are the Default Mode Network (DMN) [13], [14], [58], [59], [60], [61], Sensori-motor Network (SMN) [13], [62], [63], Executive Control Network (ECN) [15], Visual Network (VN) [13], [16], [64], [65], [66], Fronto-Parietal Network (FPN) [13], [60], [67], [68], [69], [70], Auditive Network (AN) [17], [71], [72] and Temporo-Parietal Network (TPN) [17], [72], [73]. Also, the network regions were defined according to the most reported cases, and finding their correspondence with the ROIs of DKT atlas.

4) ANATOMICAL CONSTRAINT

We selected a threshold for w_{mean}, which guaranteed that each node of the seven networks is connected, without considering of the self-connection. Under this condition, we obtained a matrix with 28% of connections, which was used to construct the reference AC with the delay matrix. In addition, AC matrices were constructed with different percentages of connections (i.e., 15%, 20%, 35%, 40%, and 100%).

[1] http://www.humanconnectomeproject.org

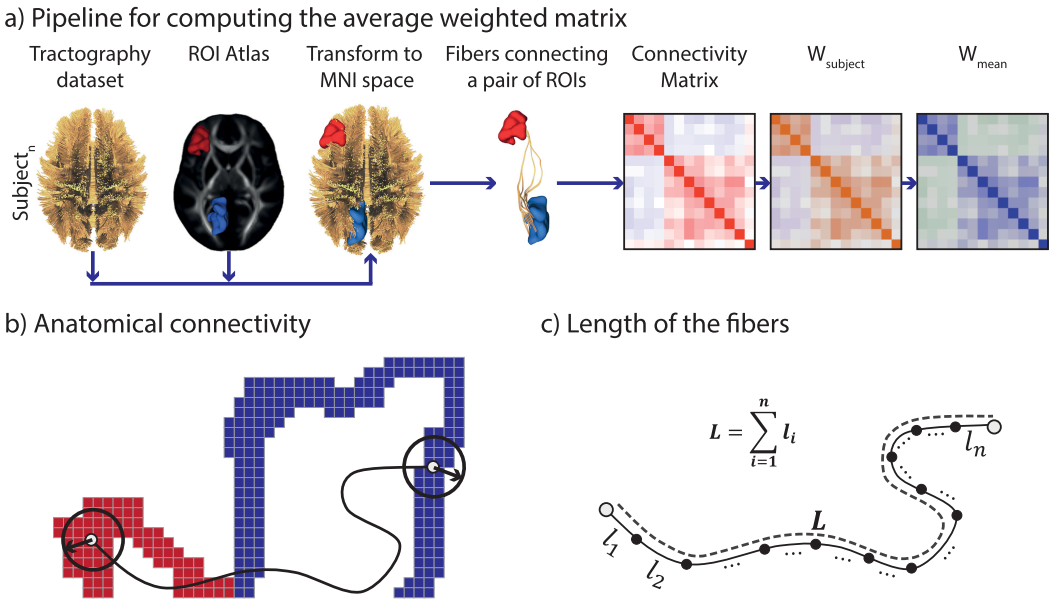

FIGURE 3. a) Calculation of the average weighted matrix w_{mean}. Subject connectivity matrices are first calculated based on the tractography dataset and anatomical ROIs in MNI space. Then, individual weighted connectivity matrices ($w_{subjecti}$) are computed based on the calculation of the connection strength (w) between each pair of ROIs. Finally, w_{mean} matrix is computed as the average of each matrix. b) Method for calculating anatomical connectivity using a radius at the ends of the fiber. c) Method for calculating the length of each fiber.

C. SIMULATIONS

Two experiments to evaluate the performance of HsMM-MAR-AC were performed. The first used synthetic data generated from a small generic system. The second used synthetic data as close as possible to the real brain functional data in terms of the magnitude and composition of the networks. It consisted of 10 non-stationary signals composed of the 7 most reported RSN in the literature. This simulation aimed to determine the limitations and advantages of the model in a real usage scenario. The methodology is explained in more detail in the following sections.

1) EXPERIMENT 1 (MODEL VALIDATION)

The first simulation generated data using a 10-node and generative HsMM-MAR-AC with a maximum delay of 3. Simulations were performed using 3, 4, and 5 states, and each state's network utilized 6 of the 10 nodes. Theses MARs were created randomly under the condition that they were stable according to the procedure explained in [74]. We used a single delay for each connection between nodes (there was only one connection per lag). We incorporated a random ranking system to establish uniform weights for the connections, and subsequently eliminated those with lower weights depending on a predetermined percentage. This allowed us to define a percentage of AC for the removal process based on the ranking. The data was performed using a 50% of AC, i. e., with 50 of 100 possible connections (10×10 nodes). Then we used the generated data to train an HSMM-MAR-AC model, which is evaluated according to Section II-D. The model was trained using different AC (25%, 50%, 75%, and 100%) and different data lengths. For each evaluation, 10 runs were executed with different MAR configurations.

2) EXPERIMENT 2 (SIMULATION AND ESTIMATION OF RSN)

Figure 1(b.4) shows the approach used to generate the realistic synthetic signals. Ten non-stationary signals were generated based on the reference connectivity (28%), which included the seven most reported RSNs; refer to Section II-B3. HsMM generative model [2] was used to generate the signals. Each network was represented by a MAR (A_i), where i is the i_{th} RSN. Each network i had a $S_{i28\%}$ matrix, which contains only the lags for the regions in network i. In addition, each network had a stable MAR process $\tilde{A}_i$ with all ROIs connected for all lags. A MAR process is stable when the module of all its eigenvalues is inferior to 1.0 [74].

The final MAR of each RSN (A_i) was obtained using the Equation 10, in which the operator $\odot$ means point-to-point multiplication. The longer average fiber was 239.8 mm. Thus, the maximum connection delay was 40 ms, and the maximum lag was $k = 8$, considering a velocity of conduction of 6 m/s and a temporal resolution of the signal $\Delta_t = 5$ ms (see Section II-B4). The DKT atlas has 62 ROIs, therefore, the dimensions for $S_{i28\%}$ were ($62 \times 62 \times 8$). The probability distribution of state duration was a Log-Normal constructed with a mean of 3.84 and 0.4% of standard deviation. These values were chosen to achieve an average state duration of 50 ms and a Log-Normal distribution with a tail extending to 150 ms, consistent with previous studies reported in the literature [28]. The transition probability matrix was designed with a non-symmetric structure, avoiding favoring particular

transition paths.

$$A_i = \tilde{A}_i \odot S_{i28\%} \tag{10}$$

Figure 1(b.5) illustrates the estimation stage, in which the signals generated in the simulation stage were used to estimate the model parameters. We used separately six different ACs (refer to Section II-B4). We increased the size of the estimated signals in steps of 120 s, from 240 s to 600 s. The initialization of the algorithm was random. The model estimated the number of states, the state sequence, the transition probability matrix, and the auto-regressors of MAR states (A_i).

D. MODEL EVALUATION

1) SIMILARITY MATRIX

The MSS similarity matrix proposed in [75] was used to evaluate the performance in estimating the MAR of each state and the transition matrix. This metric is defined in Equation (11), where M is the simulated matrix and $\hat{M}$ is the estimated one. The values range from 0 to 1, being 1 for identical matrices.

$$MSS = 1 - \frac{\| M - \hat{M} \|}{\| M \| - \| \hat{M} \|} \tag{11}$$

2) KULLBACK-LEIBLER DIVERGENCE

Analytical Kullback-Leibler divergence (KL) proposed in [76], was used to evaluate the performance of the algorithm for recovering the state duration distribution (see Equation (12)).

$$D(f_i||f_j) = \frac{1}{2\sigma_j^2}\left((\mu_i + \mu_j)^2 + \sigma_i^2 - \sigma_j^2\right) + \ln(\frac{\sigma_j}{\sigma_i}) \tag{12}$$

where f_i is the simulated state duration distribution with mean μ_i and variance σ_i; and f_j is the estimated state duration distribution with mean μ_j and variance σ_j.

3) G-TEST

G-test [77] was used to determine if the estimated duration parameters significantly differed from the design parameters (see Equation (13)).

$$G = 2\sum_i O_i \log(\frac{O_i}{E_i}) \tag{13}$$

where O_i and E_i were the observed and expected values, respectively.

E. COMPARISON WITH CURRENT METHODS OF RSN ESTIMATION

We compared the recovering of the RSNs obtained by HsMM-MAR-AC, as described above, to the estimation by the standard HMM-MAR [28]. We applied the implementation at the following link[2] and used the data described in Section II-C2 with 600 s of data duration.

[2]https://github.com/OHBA-analysis/HMM-MAR

In addition, we applied the sliding window method, which is widely used to estimate functional connectivity from fMRI data [78], [79]. We estimated the functional connectivity between the nodes of the DKT atlas [29] using Pearson correlations [80]. We used the sliding sindow approach with different window sizes: 125 ms, 250 ms, 500 ms, 1 s, and 1.50 ms, with 75% overlap. Furthermore, we tested the algorithm with the K-means [78] and Principal Component Analysis (PCA) [79] approaches for network extraction, to the data described in Section II-C2, with 600 s of data duration. In addition, we adapted the algorithm to use anatomical connectivity as a constraint, not considering the correlation between nodes that are not anatomically connected.

III. RESULTS

A. EXPERIMENT 1: MODEL VALIDATION

In this simulation, the performance of the HsMM-MAR model was evaluated using simulated data from a small network (10 nodes), a maximum lag of three, and an Anatomical Constraint (AC) of 50%. Performance evaluation was based on the training data length and the AC used in model training. In addition, the evaluation of the model was carried out considering two aspects: the verification of the parameter recovery of the original model and the evaluation of the prediction capacity of the model in new data. See Section II-D for more details of the evaluation process.

The first parameter to be evaluated is the structural type corresponding to the number of states. This parameter is crucial since its incorrect estimation involves the impossibility of recovering the other parameters of the model. For this evaluation, data with 3, 4, and 5 states (networks) and a data sequence length of 5 s and 20 s were generated. Then, based on the data, the models were trained, and the convergence curves of the models' selection were obtained, allowing us to estimate the number of states. The result of the convergence curves can be seen in Appendix B (Figure 11). Here, the HsMM-MAR model with AC correctly estimates the number of states for all cases. On the other hand, without AC, it correctly estimates the number of states only for the case of 20 s.

Two essential variables to evaluate the performance of the models are the percentage of AC and the length of the data sequences used in estimating the model parameters. For this reason, we evaluate the recovery of these parameters based on these two variables using a matrix where the color will indicate the model's performance. Therefore, the first step is to evaluate the performance of the recovery of states, which can be seen in Figure 4(a). In addition, the recovery of the MAR coefficient matrix can be seen in Figure 4(b). These figures show how using AC allows the model to provide a good performance with a much shorter data length than the case of not using AC. This is consistent with the fact that not using an AC implies estimating more parameters; therefore, more data is required.

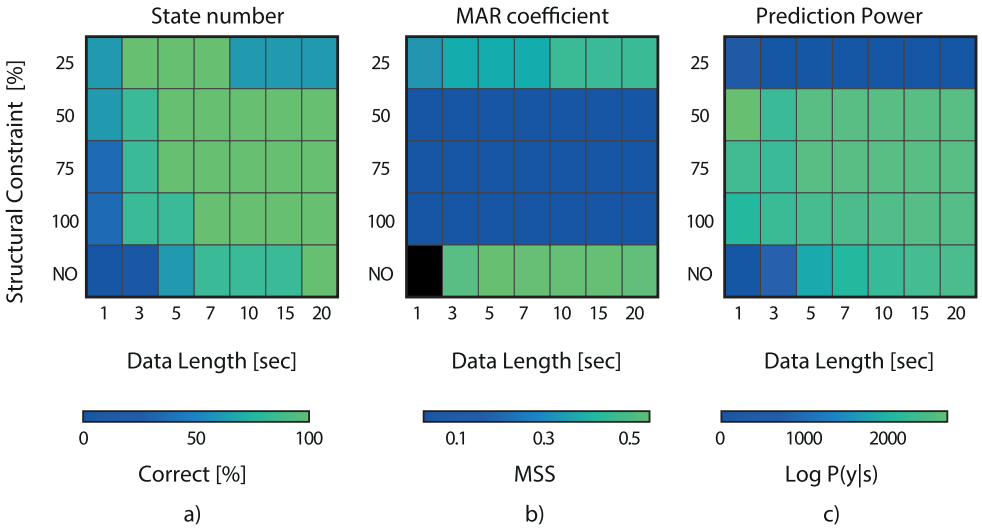

FIGURE 4. Experiment 1: Accuracy of model estimation for varying levels of Anatomical Constraints and signal durations. (a) Shows the success in recovering the correct number of states over 10 runs. With 50% AC and 5 seconds of data, the number of states is accurately estimated. To achieve the same accuracy at 100% AC (i.e., all the connections are included, each with only one lag), 7 seconds of data were needed. Without AC, the NO row, the data requirement for accurate recovery of the states increases to 20 seconds. (b) Accuracy of the estimated MAR coefficient matrix as a distance between the real and estimated (MSS). MSS, which ranges from 0 to 1, was calculated only when the number of states was accurately recovered. Performance was poor when no AC applied, or the AC was too severe (only 25% of connections were included). (c) Predictive power of the model. Predictive power is poorer without AC or with excessive AC.

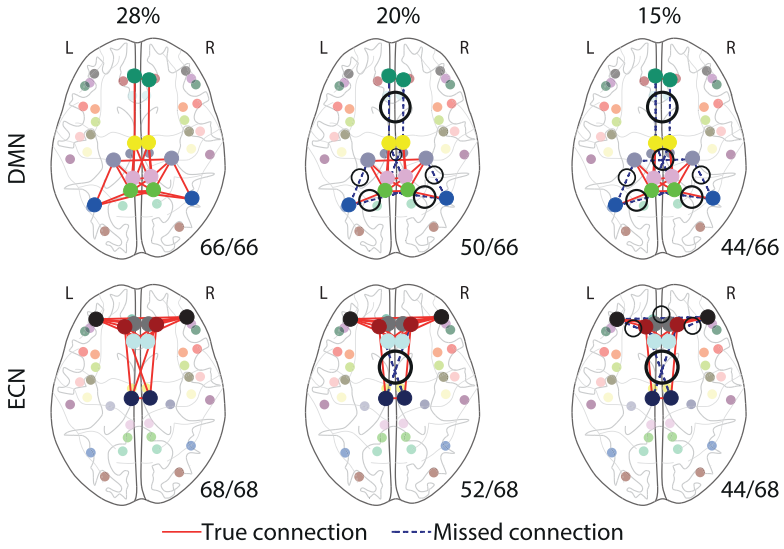

FIGURE 5. Illustration of the anatomical connections in the DMN and ECN designed for 15%, 20%, and 28% AC. For each case, the lower right corner shows the percentage of connections by respect to the reference connectivity (28%). Note the loss of connections for 15 and 20% of AC (in dashed lines).

Concerning the recovery of the parameters associated with the transition matrix and duration distribution of the models, a good performance is observed, with no differences between the different cases. To see the details of this performance, see the Appendix B (Figure 9).

Figure 4(c) shows the predictive power of the model, see Section II-D for more details about the calculations for this metric. AC allows reaching values close to the maximum prediction power with a minor data length requirement. Finally, it is also verified that the variations of AC between 50% and 100% do not significantly vary the prediction power.

B. EXPERIMENT 2: SIMULATION AND ESTIMATION OF BRAIN RESTING STATE NETWORKS

For testing the performance of HsMM-MAR, we used ACs with different percentages of connections (15%, 20%, 28%,

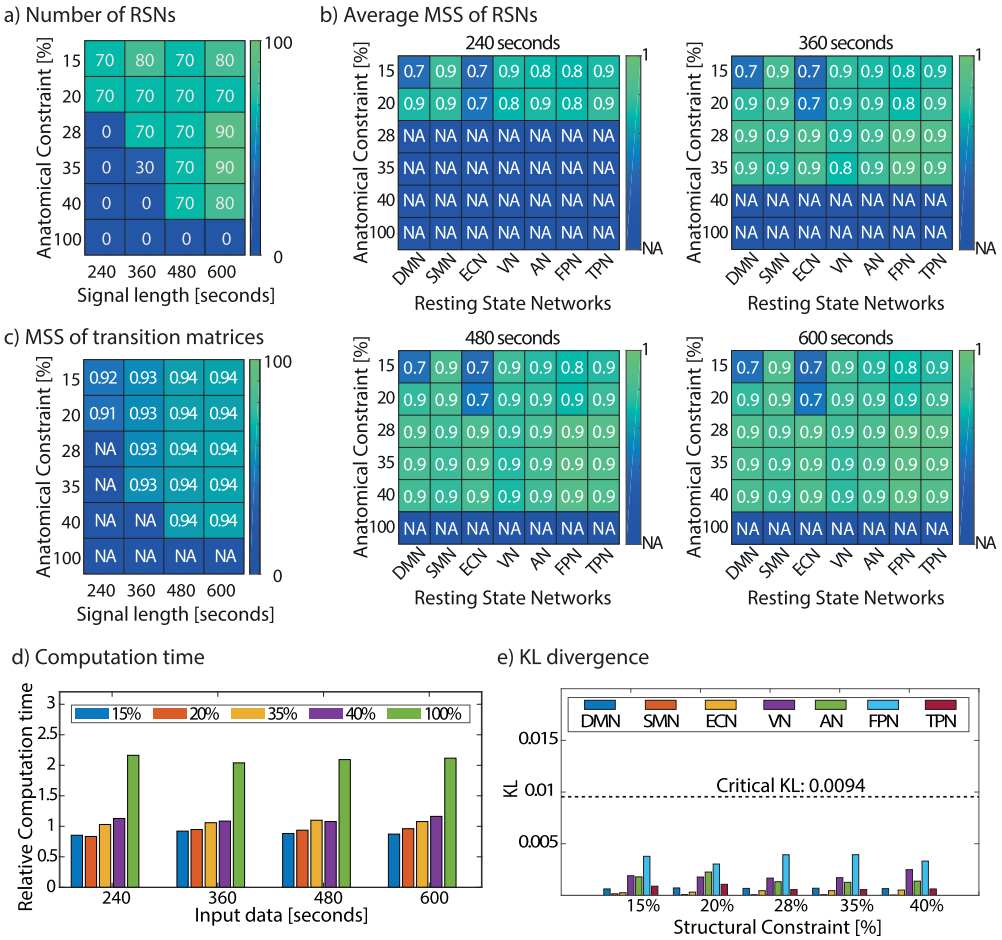

FIGURE 6. (a) Percentage of success in detecting the number of RSNs. (b) Average MSS of RSNs, varying the percentage of connections and the signal's length. (c) Average MSS of the estimated transition matrices versus the design transition matrix. (d) Estimation computation time for the different ACs with respect to the estimation time for a 28% AC. (e) KL divergence between the design duration distribution of the states for each RSN and the duration distributions calculated from the parameters estimated by the algorithm.

35%, 40%, and 100%) with 10 non-stationary signals and 5 iterations for each run. The signals were obtained using the generative HsMM-MAR with the seven most reported RSN structure (refer to Section II-B3), and signal length of 240 s, 360 s, 480 s, and 600 s. The reference AC (28%) was selected for constructing the RSNs structure, which was found by assuming that each node of each network must be connected to at least one node. We used a non-symmetric transition matrix in which probabilities avoided a preferred path. The probability duration of states was designed with a mean of 3.84 and 0.4% of standard deviation, see section II-C2. The reference AC contained 1066 connections. Under these conditions, the RSNs structure had the following number of connections: DMN (66), SMN (32), ECN (68), AN (34), VN (16), FPN (88), TPN (104). The ACs with 15%, 20%, 35%, 40% and 100% had 578, 770, 1346, 1540 and 3844 connections, respectively. The ECN and DMN networks lose connections for ACs of 15% and 20%. Figure 5 shows the connections for 15, 20 and 28% of connections. For the 15% of connections, the DMN had 44 of 66 connections, and ECN had 44 of 68 connections. For the 20% of connections, the DMN had 50 of 66 connections, and ECN had 52 of 68 connections.

The correlation between the delay and the weighted connectivity is -0.30 with a p-value < 0.01, for details, see Appendix B (Figure 12). Stronger restrictions eliminate long connections, which do not significantly affect the connections among the ROIs of the RSNs.

Figure 6(a) shows the percentage for correctly detecting the number of RSNs. HsMM-MAR was able to detect the correct number of networks with ACs of 15 and 20% of connections. For ACs larger than 20%, HsMM-MAR needed signals with at least 360 seconds. Higher accuracy was reached for larger signals and smaller connections in the ACs. Figure 6(b) shows the MSS metrics of the estimated versus simulated networks. The NA values correspond to cases where the correct number of networks was not found. Networks were matrices that represented a MAR process. Higher MSS values were found for the reference AC (28%) and larger signals. Both DMN and ECN networks had smaller MSS for ACs of 15 and

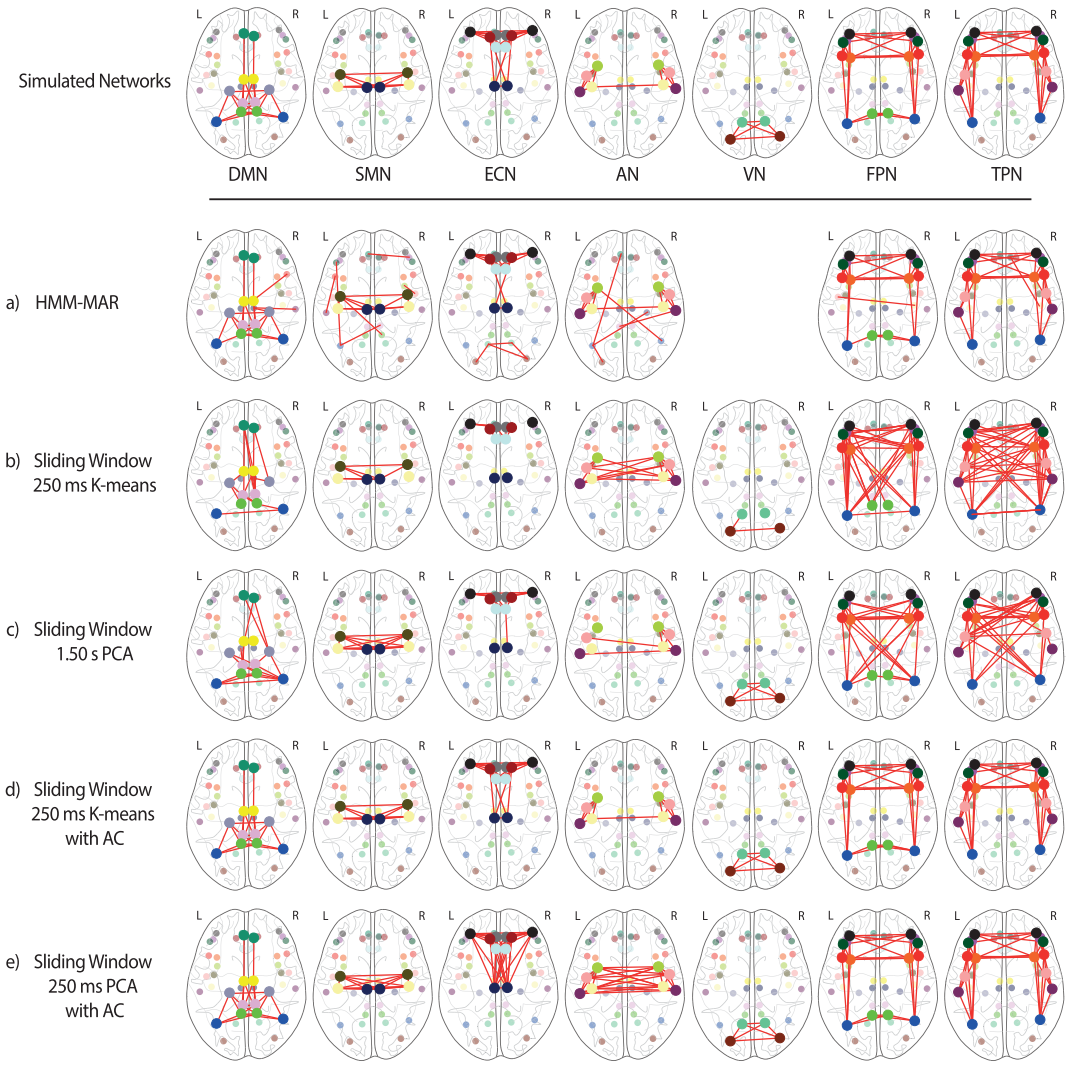

FIGURE 7. Illustration of the structure of the simulated networks and the structure of the networks that were estimated using the state-of-art algorithms. a) HMM-MAR algorithm. The algorithm automatically decides the number of detected networks, in this case it detected 6 networks. The results show that the Executive Control Network was mixed with the Visual Network. b) Sliding window algorithm with K-means.c) Sliding window algorithm with PCA. d) Sliding window algorithm with K-means with AC. e) Sliding window algorithm with PCA with AC.

20% of connections. Figure 6(c) shows the MSS metrics of the estimated versus simulated transition probability matrix. The NA values involve cases where the correct number of networks was not found. Higher metrics were obtained for larger signals.

HsMM-MAR explicitly estimated the duration of the states through a probability distribution. The states were designed with a Log-Normal duration distribution. Figure 6(e) shows the KL divergence between the recovered and design duration distributions for the RSNs, with the 600 seconds signals and varying the AC. The black dashed line indicates the critical KL distance value. All the divergences were under the critical threshold. Also, We assessed the computation time needed for estimations. The HsMM-MAR was forced to detect seven states to guarantee equality of conditions in each iteration. Figure 6(d) illustrates the estimation computation time for the different ACs, with respect to the reference AC (28%), for different signal lengths. As observed, the computation time increased with AC allowing a higher percentage of anatomical connections. In addition, we calculated the cumulative distribution function (CDF) of the state's duration to evaluate the accuracy of estimating the state duration's probability distribution. In appendix B, the figure 10 plots the function $1 - CDF$, estimated for the 600 second signals, varying the percentage of AC, for each RSN. The x-axis was in logarithmic scale. The black dashed lines indicated the cumulative distribution function obtained with the performance test (analysis performed with G-test, refer

to Section II-D), defining the reliability range. Distributions outside the reliability range are considered different from the duration distribution of the simulated signals. It can be seen that the duration probability of each estimated network did not present significant differences with the designed duration distribution.

C. COMPARISON WITH CURRENT METHODS OF RESTING STATE NETWORKS ESTIMATION

1) HMM-MAR

Figure 7(a) shows the structure of the networks extracted by the HMM-MAR algorithm. HMM-MAR can decide the number of networks it estimates. For this experiment, the algorithm estimated 6 of the 7 networks. The missing network was the VN, which was mixed with the Executive Control Network.

2) SLIDING WINDOWS

Figures 7(b) and 7(c) show the structure of the networks extracted by the sliding windows algorithm with K-means and PCA, respectively. Figures 7(d) and 7(e) show the structure of the networks extracted by the sliding windows algorithm with K-means and PCA, respectively, using the AC. The figure shows the most favorable results achieved by each algorithm, based on the window size. For recovering the networks, the sliding window with K-means achieves greater accuracy with a window size of 250 ms, and the sliding window with PCA achieves greater accuracy with a window size of 1.50 s. When using AC, both sliding window with K-means and sliding window with PCA recover networks more accurately using a window size of 250 ms.

IV. DISCUSSION AND CONCLUSION

We present an efficient method for detecting the RSNs and their dynamics using functional brain signals. Identifying these dynamic patterns has relevant applications in studying brain diseases such as Alzheimer's, Schizophrenia, Epilepsy, and brain lesions [21]. The temporal dynamics of brain networks are modeled with a generative HsMM model that allows the modeling of state duration through probability distributions. In addition, each network is characterized by a MAR, enabling the spectral analysis of the network and the temporal interactions between its ROIs. The MARs were constrained using anatomical connectivity and the connection delay between ROIs. These constraints were extracted using diffusion MRI data from the HCP database. Both anatomical connectivity and connection delays were represented jointly using a sparse matrix considering the connection delay between ROIs. The performance of the algorithm was first evaluated using a simple simulation with 10 nodes to validate the correct implementation of the model. Next, we used a more complex simulation based on 62 anatomical ROIs and the 7 most reported RSNs. In both experiments, we assessed the algorithm's performance for detecting the number of networks, the state duration distributions, and the sequence of states for the simulated signals, using different ACs and signal lengths. We used simulated signals because there is no gold standard in real signals. RSNs emerge as hidden states that an expert cannot observe. Therefore, it is impossible to measure the proposed method's performance with real signals.

The first experiment validated the model implementation's correct functioning, integrating connectivity constraint and connection delay information to the HsMM-MAR model. It is verified that the model can recover the correct number of states using the free energy curve and recover the other parameters correctly.

The second experiment demonstrated that the AC with a low percentage of connections enabled faster algorithm convergence, even for short signals. On the other hand, when we used all the connections (100% of connections), the algorithm could not estimate the correct numbers of RSNs, for the simulated signal lengths. Note that a 100% of AC contains all the connections but only one delay per connection, which is still a sparse matrix. If we do not use the AC, the delay matrix is full, and the algorithm is not computationally feasible. Compared to the 100% of AC, the reference connectivity (28% of connections) reduces the effort of the model, requiring shorter signals. Furthermore, it reduces the computational cost by around 2 times. In addition, the results also demonstrated the algorithm's robustness since, over a minimum signal length for a given constraint, it showed a stable behavior.

Moreover, the state duration parameters were recovered with high accuracy when the algorithm correctly detected the number of states. For these cases, the estimated transition probability matrices had a MSS by respect to the design matrices greater than 0.91. In addition, the KL divergence and the G-test between the recovered and design duration distributions showed that the state duration parameters were obtained with a wide confidence interval for all RSNs.

Functional brain data are time series; therefore, they can be modeled by a Multivariate Autoregressive Regression (MAR) model. Other data-driven methods can be used to analyze time series. The research of [81] compares different measures of data-driven methods on simulated data by using three systems (Hénon maps, MARs, and simulated EEG). They reported that no measure shows superior performance. However, MARs are helpful because they perform spectral signal analysis. Also, several studies have used these models to analyze fMRI signals. The work of [46] was the first group to apply MAR to model fMRI signals. A multi-scale generative model for EEG was proposed in [82], which assumes that a MAR model can model the mesostates. However, they characterize the mesostates as stationary. Therefore [1] proposed adding a level of flexibility by using temporal clusters characterized by MAR models. Nevertheless, it is impossible to obtain a transition probability between mesostates with this approach. Subsequently, [35] proposed a method for source reconstruction with a MAR model representing interactions

among brain regions, defining the model order based on the connection lag.

Previous studies did not consider the dynamics of brain activity in estimating the models. Using a Hidden Markov Model (HMM), it is possible to define the observation model as a MAR, as proposed by [28]. However, in HMM, the distributions of state durations are geometric, assigning high probabilities to faster changes among states. In this regard, [83] demonstrated that a Markov process's Auto Information Function (AIF) differs critically from an AIF of the real data. Hence, the Hidden semi-Markov Model (HsMM) arises as an excellent tool to model the distribution of state duration [2]. Nevertheless, the MAR observation model may be excessively complex and computationally unapproachable.

The number of parameters to estimate can be calculated as $(n \times n \times d)$, where n is the number of nodes and d is the order of the MAR. In addition, complex models can suffer from overfitting. This occurs when the model cannot correctly generalize from the training data and performs poorly for the testing data [31]. In some cases, overfitting occurs by building a model with little data for training in relation to the number of parameters to be estimated [30], [31]. As a result, the model may be unidentifiable in extreme cases when the training set needs to be larger to converge to a single solution. In these cases, it is possible to apply model constraints to reduce the parameters to be estimated [84]. For this reason, we proposed an HsMM-MAR-AC approach that allows a considerable reduction in the parameters to be estimated.

Functional integration between different areas in the brain is mediated by White Matter (WM) connections [34]. The study of [38] found that high anatomical connectivity involves high functional connectivity. Later, several studies have reported that functional dynamics reflect anatomical connectivity [39]. These findings suggest that anatomical connectivity can be used as a constraint in studying functional connectivity. In works such as [44], [45], and [35], anatomical connectivity is applied as a constraint to MAR models of high complexity. Recently, in [85], an autoregressive model was used for studying the association between anatomical connectivity and functional brain activity by using a multi-lag autoregressive constrained for the AC. They studied the relationship between the structure and functionality of the brain. They found that effective connectivity better describes the functional interactions, keeping the original anatomical organization and discriminating between cases and controls.

The authors used the Akaike information criterion [86] for defining the MAR order. We determined the MAR order based on the maximum fiber length. On the other hand, in [35] an arbitrary threshold was applied to define the AC. In our work, we used the average weighted connectivity matrix (Equation 9) for thresholding the AC.

The AC discards the weakest connections, which may cause the loss of some RSN connections. In this work, we used a reference threshold, where all the RSN connections are preserved, leading to a connectivity matrix with 28% connections. In addition, most restrictive ACs eliminate some long (a higher proportion of long connections than short) connections of the whole matrix. This behavior suggests that the connection weights are stronger for short connections in RSNs. However, the correlation between the delay matrix and the average weighted connectivity matrix is low (-0.30). This occurs because very long connections are not important in RSNs, which have low connection weights.

When removing connections of some RSNs, the MSS between the simulated and estimated networks is lower for the affected networks. However, even if connections are lost, it is possible to provide with high accuracy, both the temporal dynamics of the networks and the probability of state transition. In addition, shorter signals are needed to obtain the dynamics, which is relevant since the functional activity is generally measured by short signals., and In many cases, it is required to concatenate signals from several subjects. We may avoid the loss of connections by using a 100% AC. However, the accuracy for recovering the number of RSNs decreases to 40%. Besides, the MSS between the simulated and estimated networks decreases, requiring larger signals to obtain the same performance as constraints with fewer connections. The best performance is obtained for the reference connectivity (28%), which demonstrates the relevance of validating a method to assess the accuracy for obtaining the optimal AC. Finally, it is possible to use only the RSN connections. In this scenario, the performance of the algorithm should be better. However, to avoid introducing a bias, we were as objective as possible in defining the thresholds of the ACs guided by the biological information (connection weight).

Finally, we compare the performance of the proposed algorithm with the most commonly used algorithms in the state-of-the-art. We used the HMM-MAR algorithm [3], [28], which is the current standard, with our simulated signals and without AC. The results can be seen in Figure 7(a), which shows that HMM-MAR is not able to retrieve the number of states. However, HMM finds the structure of the networks. The Visual Network is mixed with the Executive Control Network; this behavior can be avoided using longer signals. Another way to avoid omitting networks is to adapt the algorithm to use the AC matrix, as it has proven useful in HsMM. On the other hand, HMM-MAR, unlike HsMM-MAR, can converge without using the AC. However, HMM-MAR cannot correctly estimate the duration of states because they are inherently modeled by a geometric distribution, which differs significantly from a Log-Normal distribution. In addition, we used the sliding window approach using K-means and PCA. The results show that this approach is able to detect the structure of the networks. However, the sliding window approach has the disadvantage of a priori choice of window size. Very small windows may provide spurious activities among ROIs, and very large windows may omit functional activity. Another disadvantage is that this approach makes it impossible to model the states' duration.

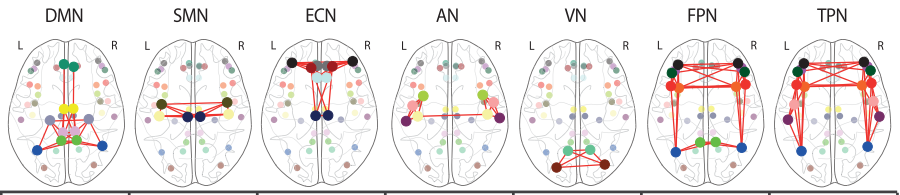

	DMN	SMN	ECN	AN	VN	FPN	TPN
CAM			X				
CMF							X
InfP	X						X
InfT							
IC	X						
LOcc					X		
LinG					X		
MOrb	X						
MT				X			
PH	X						
PCen		X	X				
POper							X
POrb							X
PTria							X
PostC		X		X			
PostCin	X						
Prec		X					
PCun	X						
RAC			X				
RMF			X				X
SupF			X				
SupT				X			
Ins				X			

FIGURE 8. Nodes of the Resting State Networks [RSN] based on the Desikan-Killiany atlas thresholded at 28% of all anatomical connections as described in Section II-B4, which conserved all RSNs. Abrreviations: CAM (Caudal Anterior Cingulate), CMF (Caudal Middle Frontal), CN (Cuneus), ENT (Entorhinal), FUS (Fusiform), InfP (Inferior Parietal), InfT (Inferior Temporal), IC (Isthmus Cingulate), LOcc (Lateral Occipital), LOrb (Lateral Orbitofrontal), LinG (Lingual), MOrb (Medial Orbitofrontal), MT (Middle Temporal), PH (Parahippocampal), PCen (Paracentral), POper (Pars Opercularis), POrb (Pars Orbitalis), PTria (Pars Triangularis), Pcal (Pericalcarine), PostC (Postcentral), PostCin (Posterior Cingulate), Prec (Precentral), PCun (Precuneus), RAC (Rostral Anterior Cingulate), RMF (Rostral Middle Frontal), SupF (Superior Frontal), SupP (Superior Parietal), SupT (Superior Temporal), Supra (Supramarginal), TT (Transverse Temporal), Ins (Insula).

In order to test the advantages of the AC, we adapted the AC to apply to the sliding window approach. Applying the AC improves the results of losing connections or maintaining spurious connections. The largest differences are obtained in the DMN and the parietal networks (FPN and TPN). Although the AC improves the results, it is necessary to adapt it for this type of algorithm by disregarding the information of the connection delay contained in the AC. This may represent a disadvantage because the connection delay information has the potential to reveal the workings of functional dynamics in the brain.

In real data, the delay of connections may be variable among different people due to diseases [87], aging, or the natural development of brain connections resulting from their experiences. However, [87] modeled the conduction delays in the corpus callosum and did not find differences with age. In our work, we used a single delay for each connection, which may be a simplistic approach. Nevertheless, we used 5 ms of temporal resolution; thus, we may assume that the sample rate absorbs the delay variability.

A significant aspect to consider in the connection delay representation is the number of ROIs to characterize the networks. If more ROIs are used, we may obtain better descriptions of the interactions. However, it may be required to use very restrictive AC due to the increased model complexity. In any case, we used an ROI atlas extensively used in the literature. In addition, our approach has the flexibility to add an autoregressive if the parcellation is considered to have multimodal regions. This occurs when a region consider several nodes that can be separated with more fined-grained parcellations. Future work could explore different atlases and evaluate the impact of the atlas selection.

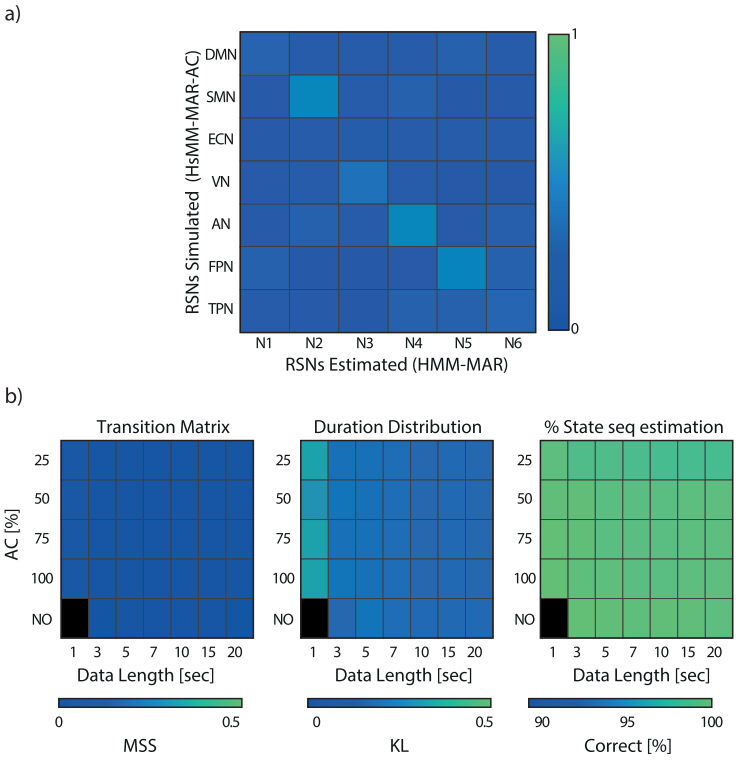

FIGURE 9. a) Illustration of the MSS of the simulated networks versus the networks estimated with HMM using a 600-second signal. The *x*-axis shows the networks estimated by HMM-MAR, and the *y*-axis shows the simulated networks. HMM, without anatomical constraint, is not able to detect the 7 states present in the simulated non-stationary signal. The results show that the networks do not recover correctly. (b) In the three graphs, the *y*-axis indicates the % of AC used, and the *x*-axis the duration in seconds of experiment 1 (Section III-A). Left panel shows the recovery performance of the transition matrix by means of the MSS distance between the real matrix and the estimated one. The range of this metric is from 0 to 1, and it was obtained only for those cases where the number of states was correctly determined. The black color indicates that it is not possible to calculate this metric because there are no cases where it converges to the correct number of states. In most cases, the recovery is very good, resulting in values around 0. Center panel shows the recovery performance of the durations distribution by means of the KL distance between the real distribution and the estimated one. In most cases, the recovery is very good, resulting in values around 0.1. Right panel shows the % recovery of the state sequence. In most cases, the recovery is very good, resulting in values around 98%.

The results prove the impact of the AC on the algorithm's performance. The accuracy of estimating the number of states decreases with a more relaxed AC. Obtaining a better performance would require longer signals and estimation times. In any case, AC turns the effort of the algorithm computationally approachable. For more restrictive constraints that lead to the loss of some RSN connections, the algorithm can still recognize all 7 RSNs, which shows the algorithm's robustness to errors in the definition of AC. Furthermore, the accuracy in estimating the state duration distributions demonstrates a correct estimation of the signal dynamics.

The proposed method enables an efficient and feasible tool to analyze brain dynamics. In addition, using AC can improve the performance of other algorithms, such as sliding windows. The data used in this work are freely available at the following link.[3]

[3]https://u.pcloud.link/publink/show?code=kZRPYBVZn1CFk5iJGtjRvdrdh2JVwk1hvRrX

APPENDIX A
VARIATIONAL BAYES INFERENCE

In order to infer the parameters of the model, we utilize the variational approach [2], [30], which requires alternating between an E-step and an M-step. The E-step is responsible for estimating the probabilities of the hidden states, while the M-step estimates the model parameters. This type of algorithm ensures convergence and can be tracked using the model's free energy. To begin, we will outline the M-step.

A.1. M-Step

a) W Coefficient MAR

$$q(w_{nl_n}^{(k)}) = (N(w_{nl_n}^{(k)}|\bar{w}_{nl_n}^{(k)}, \Upsilon_n^{(k)^{-1}}) \tag{14}$$

With:

$$\bar{w}_{nl_n}^{(k)} = \sum_{t=1}^{T} \gamma_t^{(k)} \times \bar{\phi}_n^{(k)} \times \Upsilon_n^{(k)^{-1}} \times {x_{l_n t}}^T \times y_{nt} \tag{15}$$

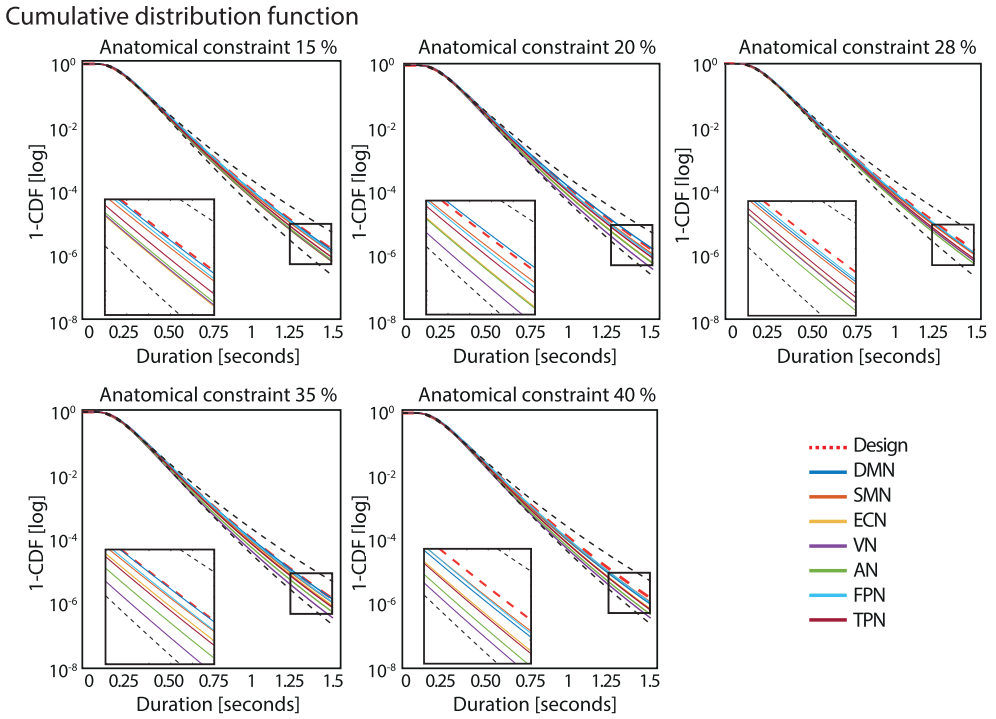

FIGURE 10. The plots display 1-CDF for the states of the seven RSNs, where CDF is the cumulative distribution function of the state duration, estimated by the algorithm, varying the AC for a signal size of 600 seconds. The red dashed lines indicate the design CDF, the continuous lines show the CDF for the different RSNs, and the black dashed lines delimit the reliability area. The *y*-axis is on a logarithmic scale.

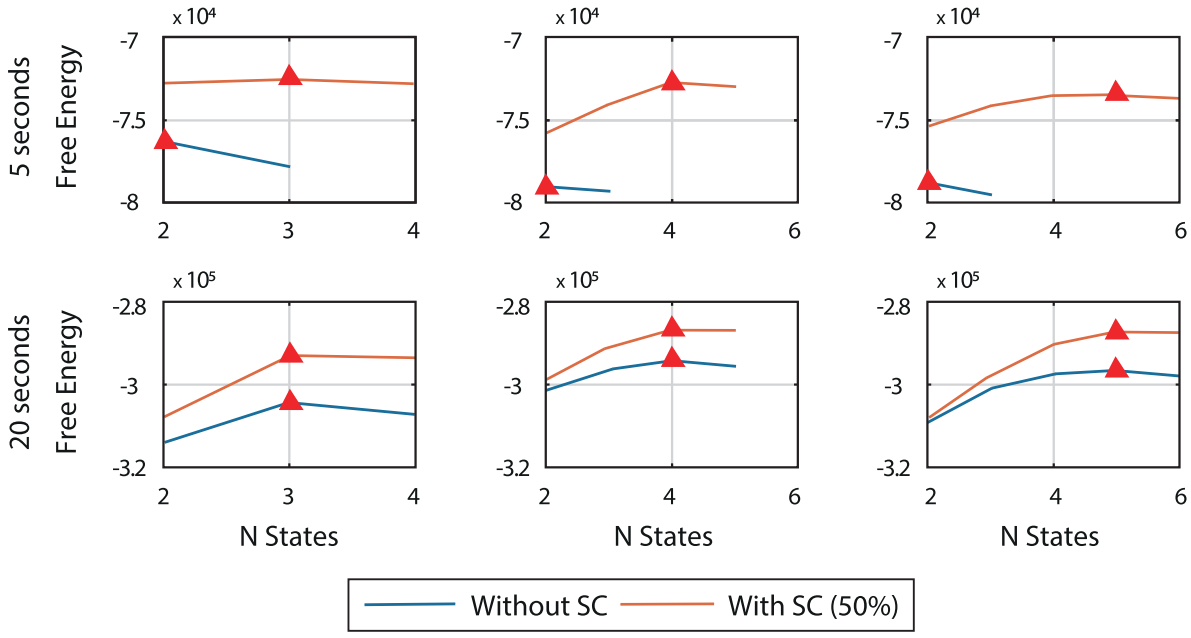

FIGURE 11. Free Energy convergence curve in training: The estimated number of states corresponds to the maximum of the Free Energy function, in this case marked with the figure of a red triangle. Each graph shows the curve with the model with and without the use of RE.

$$\Upsilon_n^{(k)} = \left(\sum_{t=1}^{T} \gamma_t^{(k)} \times \bar{\lambda}_{nl_n}^{(k)} \times \bar{\phi}_n^{(k)} \times x_{l_n t} \times x_{l_n t}{}^T\right)^{-1} \tag{16}$$

where $\bar{w}_{nl_n}^{(k)}$ and $\Upsilon_n^{(k)}$ correspond to the mean and Precision of Normal distribution, $\gamma_t^{(k)}$ corresponds to the probability that state k is active at time t, which is obtained in E-Step.

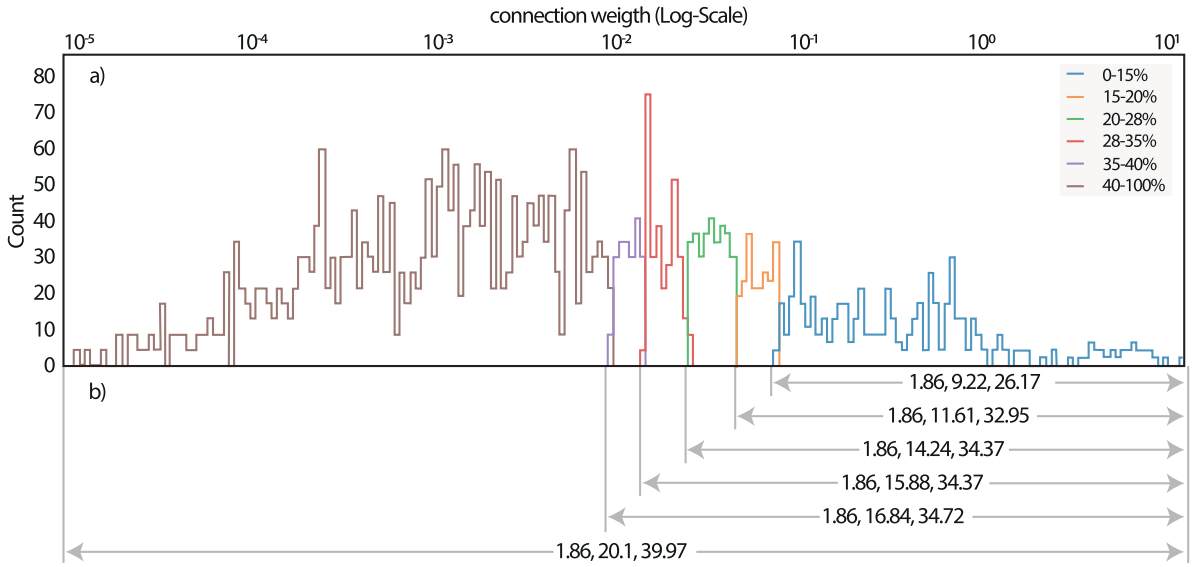

FIGURE 12. (a) Histogram of the connection weight. The colors show the histogram of the different AC. (b) The minimum, mean and maximum value of the connection delay (in millimeters) corresponding to each AC. With stronger restrictions, some long connections were lost. However, with the 15% AC, only short connections of the ECN and DMN were lost.

b) MAR Coefficient Precision

$$q(\lambda_{nj}^{(k)}) = Gam(\lambda_{nj}^{(k)}|b_{nj}^{(k)}, c_{nj}^{(k)}) \tag{17}$$

With:

$$b_{nj}^{(k)} = \hat{b}_{nj} + \frac{1}{2} \tag{18}$$

$$c_{nj}^{(k)} = \left(\frac{1}{\hat{c}_{nj}} + \frac{1}{2} \times \left(\bar{w}_n^{(k)^T} \times \bar{w}_n^{(k)} + Tr(\Upsilon_n^{(k)})\right)\right)^{-1} \tag{19}$$

where $b_{nj}^{(k)}$ and $c_{nj}^{(k)}$ correspond to the shape and scale of Gamma distribution.

c) Observation Noise Precision

$$q(\phi_n^{(k)}) = Gam(\phi_n^{(k)}|e_n^{(k)}, f_n^{(k)}) \tag{20}$$

With:

$$e_n^{(k)} = \hat{e}_n + \frac{\sum_{t=1}^{N} \gamma_t^{(k)}}{2}$$

$$f_n^{(k)} = \left\{\frac{1}{\hat{f}_n} + \sum_{t=1}^{N} \frac{1}{2} \times \gamma_t^{(k)} \times \left((y_{nt} - \bar{w}_{nl_n}^{(k)^T} \times x_{l_n t}\right)^2 + x_{l_n t}{}^T \times \Upsilon_n^{(k)^{-1}} \times x_{l_n t}\right)\right\}^{-1} \tag{21}$$

where $e_n^{(k)}$ and $f_n^{(k)}$ correspond to the shape and scale of Gamma distribution.

A.2. E-Step

To estimate the probabilities of the HMM hidden state sequence in the variational E-step of the algorithm, we can use regular forward-backward recursions [2]. This process requires the calculation of conditional likelihoods.

$$P(y_t|W, \Phi, s_t, \tau_t) = exp(\sum_{t=1}^{N} -\frac{1}{2} \times log(2 \times \pi) - \frac{1}{2} \times (\Psi(e_n^{(k)}) + log(f_n^{(k)})) - \frac{1}{2} \times ((y_{nt} - \bar{w}_{nl_n}^{(k)^T} \times x_{l_n t})^2 + x_{l_n t}{}^T \times \Phi_n^{(k)^{-1}} \times x_{l_n t}) \tag{22}$$

where Ψ corresponds to the Digamma function.

APPENDIX B
SUPPLEMENTARY IMAGES

See Figs. 8–12.

ACKNOWLEDGMENT

(Hernan Hernandez Larzabal and David Araya contributed equally to this work.)

HCP Data were provided by the Human Connectome Project, WUMinn Consortium (Principal Investigators: David Van Essen and Kamil Ugurbil; 1U54MH091657), funded by the 16 NIH Institutes and Centers that support the NIH Blueprint for Neuroscience Research; and by the McDonnell Center for Systems Neuroscience at Washington University.

REFERENCES

[1] I. Olier, N. J. Trujillo-Barreto, and W. El-Deredy, "A switching multi-scale dynamical network model of EEG/MEG," *NeuroImage*, vol. 83, pp. 262–287, Dec. 2013.

[2] N. J. Trujillo-Barreto, D. Araya, and W. El-Deredy, "The discrete logic of the brain—Explicit modelling of brain state durations in EEG and MEG," *bioRxiv*, 2019, Art. no. 635300.

[3] D. Vidaurre, R. Abeysuriya, R. Becker, A. J. Quinn, F. Alfaro-Almagro, S. M. Smith, and M. W. Woolrich, "Discovering dynamic brain networks from big data in rest and task," *NeuroImage*, vol. 180, pp. 646–656, Oct. 2018.

[4] A. Khanna, A. Pascual-Leone, C. M. Michel, and F. Farzan, "Microstates in resting-state EEG: Current status and future directions," *Neurosci. Biobehavioral Rev.*, vol. 49, pp. 105–113, Feb. 2015.

[5] G. C. O'Neill, P. Tewarie, D. Vidaurre, L. Liuzzi, M. W. Woolrich, and M. J. Brookes, "Dynamics of large-scale electrophysiological networks: A technical review," *NeuroImage*, vol. 180, pp. 559–576, Oct. 2018.

[6] M. W. Woolrich, A. Baker, H. Luckhoo, H. Mohseni, G. Barnes, M. Brookes, and I. Rezek, "Dynamic state allocation for MEG source reconstruction," *NeuroImage*, vol. 77, pp. 77–92, Aug. 2013.

[7] P. Ritter, V. K. Jirsa, A. R. McIntosh, and M. Breakspear, "Editorial: State-dependent brain computation," *Frontiers Comput. Neurosci.*, vol. 9, p. 77, Jun. 2015.

[8] M. Wang, B. Jie, W. Bian, X. Ding, W. Zhou, Z. Wang, and M. Liu, "Graph-kernel based structured feature selection for brain disease classification using functional connectivity networks," *IEEE Access*, vol. 7, pp. 35001–35011, 2019.

[9] J. A. Contreras, V. Aslanyan, M. D. Sweeney, L. M. J. Sanders, A. P. Sagare, B. V. Zlokovic, A. W. Toga, S. D. Han, J. C. Morris, A. Fagan, P. Massoumzadeh, T. L. Benzinger, and J. Pa, "Functional connectivity among brain regions affected in Alzheimer's disease is associated with CSF TNF-α in APOE4 carriers," *Neurobiol. Aging*, vol. 86, pp. 112–122, Feb. 2019.

[10] Y. Luo, Q. Tian, C. Wang, K. Zhang, C. Wang, and J. Zhang, "Biomarkers for prediction of schizophrenia: Insights from resting-state EEG microstates," *IEEE Access*, vol. 8, pp. 213078–213093, 2020.

[11] J. Li, Z. Yao, M. Duan, S. Liu, F. Li, H. Zhu, Z. Xia, L. Huang, and F. Zhou, "MuscNet, a weighted voting model of multi-source connectivity networks to predict mild cognitive impairment using resting-state functional MRI," *IEEE Access*, vol. 8, pp. 174023–174031, 2020.

[12] C. T. Briels, C. J. Stam, P. Scheltens, S. Bruins, I. Lues, and A. A. Gouw, "In pursuit of a sensitive EEG functional connectivity outcome measure for clinical trials in Alzheimer's disease," *Clin. Neurophysiol.*, vol. 131, no. 1, pp. 88–95, Jan. 2020.

[13] E. S. Finn, X. Shen, D. Scheinost, M. D. Rosenberg, J. Huang, M. M. Chun, X. Papademetris, and R. T. Constable, "Functional connectome fingerprinting: Identifying individuals using patterns of brain connectivity," *Nature Neurosci.*, vol. 18, no. 11, pp. 1664–1671, Nov. 2015.

[14] R. L. Buckner and L. M. DiNicola, "The brain's default network: Updated anatomy, physiology and evolving insights," *Nature Rev. Neurosci.*, vol. 20, no. 10, pp. 593–608, Oct. 2019.

[15] W. W. Seeley, V. Menon, A. F. Schatzberg, J. Keller, G. H. Glover, H. Kenna, A. L. Reiss, and M. D. Greicius, "Dissociable intrinsic connectivity networks for salience processing and executive control," *J. Neurosci.*, vol. 27, no. 9, pp. 2349–2356, Feb. 2007.

[16] W. D. Stevens, R. L. Buckner, and D. L. Schacter, "Correlated low-frequency BOLD fluctuations in the resting human brain are modulated by recent experience in category-preferential visual regions," *Cerebral Cortex*, vol. 20, no. 8, pp. 1997–2006, Aug. 2010.

[17] M. van den Heuvel, R. Mandl, and H. H. Pol, "Normalized cut group clustering of resting-state fMRI data," *PLoS ONE*, vol. 3, no. 4, p. e2001, Apr. 2008.

[18] D. J. Lurie, "Questions and controversies in the study of time-varying functional connectivity in resting fMRI," *Netw. Neurosci.*, vol. 4, no. 1, pp. 30–69, Jan. 2020.

[19] R. Liégeois, J. Li, R. Kong, C. Orban, D. Van De Ville, T. Ge, M. R. Sabuncu, and B. T. T. Yeo, "Resting brain dynamics at different timescales capture distinct aspects of human behavior," *Nature Commun.*, vol. 10, no. 1, p. 2317, May 2019.

[20] S. A. Cutts, J. Faskowitz, R. F. Betzel, and O. Sporns, "Uncovering individual differences in fine-scale dynamics of functional connectivity," *Cerebral Cortex*, vol. 33, no. 5, pp. 2375–2394, Feb. 2023.

[21] E. C. A. Hansen, D. Battaglia, A. Spiegler, G. Deco, and V. K. Jirsa, "Functional connectivity dynamics: Modeling the switching behavior of the resting state," *NeuroImage*, vol. 105, pp. 525–535, Jan. 2015.

[22] G. C. O'Neill, P. K. Tewarie, G. L. Colclough, L. E. Gascoyne, B. A. E. Hunt, P. G. Morris, M. W. Woolrich, and M. J. Brookes, "Measurement of dynamic task related functional networks using MEG," *NeuroImage*, vol. 146, pp. 667–678, Feb. 2017.

[23] A. Mheich, M. Hassan, M. Khalil, C. Berrou, and F. Wendling, "A new algorithm for spatiotemporal analysis of brain functional connectivity," *J. Neurosci. Methods*, vol. 242, pp. 77–81, Mar. 2015.

[24] M. G. Preti, T. A. Bolton, and D. Van De Ville, "The dynamic functional connectome: State-of-the-art and perspectives," *NeuroImage*, vol. 160, pp. 41–54, Oct. 2017.

[25] L. A. Baccalá and K. Sameshima, "Partial directed coherence: A new concept in neural structure determination," *Biol. Cybern.*, vol. 84, no. 6, pp. 463–474, May 2001.

[26] M. Kamiński, M. Ding, W. A. Truccolo, and S. L. Bressler, "Evaluating causal relations in neural systems: Granger causality, directed transfer function and statistical assessment of significance," *Biol. Cybern.*, vol. 85, no. 2, pp. 145–157, Aug. 2001.

[27] L. Harrison, W. D. Penny, and K. Friston, "Multivariate autoregressive modeling of fMRI time series," *NeuroImage*, vol. 19, no. 4, pp. 1477–1491, Aug. 2003.

[28] D. Vidaurre, A. J. Quinn, A. P. Baker, D. Dupret, A. Tejero-Cantero, and M. W. Woolrich, "Spectrally resolved fast transient brain states in electrophysiological data," *NeuroImage*, vol. 126, pp. 81–95, Feb. 2016.

[29] A. Klein and J. Tourville, "101 labeled brain images and a consistent human cortical labeling protocol," *Frontiers Neurosci.*, vol. 6, p. 171, Dec. 2012.

[30] C. M. Bishop, *Pattern Recognition and Machine Learning* (Information Science and Statistics). Cham, Switzerland: Springer, 2006.

[31] X. Ying, "An overview of overfitting and its solutions," *J. Phys., Conf.*, vol. 1168, Feb. 2019, Art. no. 022022.

[32] J. D. Hamilton, *Time Series Analysis*. Princeton, NJ, USA: Princeton Univ. Press, 1994.

[33] K. V. Mardia, J. T. Kent, and J. M. Bibby, *Multivariate Analysis*. London, U.K.: Academic Press, 1979.

[34] S. N. Sotiropoulos and A. Zalesky, "Building connectomes using diffusion MRI: Why, how and but," *NMR Biomed.*, vol. 32, no. 4, p. e3752, Apr. 2019.

[35] M. Fukushima, O. Yamashita, T. R. Knösche, and M.-A. Sato, "MEG source reconstruction based on identification of directed source interactions on whole-brain anatomical networks," *NeuroImage*, vol. 105, pp. 408–427, Jan. 2015.

[36] O. Sporns, G. Tononi, and G. M. Edelman, "Connectivity and complexity: The relationship between neuroanatomy and brain dynamics," *Neural Netw.*, vol. 13, nos. 8–9, pp. 909–922, Nov. 2000.

[37] K. E. Stephan, C. Hilgetag, G. A. P. C. Burns, M. A. O'Neill, M. P. Young, and R. Kotter, "Computational analysis of functional connectivity between areas of primate cerebral cortex," *Phil. Trans. Roy. Soc. London. B, Biol. Sci.*, vol. 355, no. 1393, pp. 111–126, Jan. 2000.

[38] M. A. Koch, D. G. Norris, and M. Hund-Georgiadis, "An investigation of functional and anatomical connectivity using magnetic resonance imaging," *NeuroImage*, vol. 16, no. 1, pp. 50–241, May 2002.

[39] J. S. Damoiseaux and M. D. Greicius, "Greater than the sum of its parts: A review of studies combining structural connectivity and resting-state functional connectivity," *Brain Struct. Function*, vol. 213, no. 6, pp. 525–533, 2009.

[40] Y. Wang, X. Chen, B. Liu, W. Liu, and R. M. Shiffrin, "Understanding the relationship between human brain structure and function by predicting the structural connectivity from functional connectivity," *IEEE Access*, vol. 8, pp. 209926–209938, 2020.

[41] T. T. Nakagawa, V. K. Jirsa, A. Spiegler, A. R. McIntosh, and G. Deco, "Bottom up modeling of the connectome: Linking structure and function in the resting brain and their changes in aging," *NeuroImage*, vol. 80, pp. 318–329, Oct. 2013.

[42] G. Deco, M. L. Kringelbach, V. K. Jirsa, and P. Ritter, "The dynamics of resting fluctuations in the brain: Metastability and its dynamical cortical core," *Sci. Rep.*, vol. 7, no. 1, p. 3095, Jun. 2017.

[43] J. Cabral, M. L. Kringelbach, and G. Deco, "Functional connectivity dynamically evolves on multiple time-scales over a static structural connectome: Models and mechanisms," *NeuroImage*, vol. 160, pp. 84–96, Oct. 2017.

[44] W. D. Penny, N. J. Trujillo-Barreto, and K. J. Friston, "Bayesian fMRI time series analysis with spatial priors," *NeuroImage*, vol. 24, no. 2, pp. 350–362, Jan. 2005.

[45] M. Fukushima, O. Yamashita, T. R. Knosche, and M.-A. Sato, "MEG source reconstruction constrained by diffusion MRI based whole brain dynamical model," in *Proc. IEEE 10th Int. Symp. Biomed. Imag.*, Apr. 2013, pp. 1002–1005.

[46] W. D. Penny and S. J. Roberts, "Bayesian multivariate autoregressive models with structured priors," *IEE Proc. Vis., Image Signal*, vol. 149, no. 1, pp. 33–41, Feb. 2002.

[47] S. J. Roberts and W. D. Penny, "Variational Bayes for generalized autoregressive models," *IEEE Trans. Signal Process.*, vol. 50, no. 9, pp. 2245–2257, Sep. 2002.

[48] M. Beal, "Variational algorithms for approximate Bayesian inference," Ph.D. dissertation, Gatsby Comput. Neurosci. Unit, Univ. College London, London, U.K., 2003.

[49] M. I. Jordan, Z. Ghahramani, T. S. Jaakkola, and L. K. Saul, "An introduction to variational methods for graphical models," *Mach. Learn.*, vol. 37, no. 2, pp. 183–233, Nov. 1999.

[50] J.-D. Tournier, F. Calamante, and A. Connelly, "Robust determination of the fibre orientation distribution in diffusion MRI: Non-negativity constrained super-resolved spherical deconvolution," *NeuroImage*, vol. 35, no. 4, pp. 1459–1472, May 2007.

[51] R. E. Smith, J.-D. Tournier, F. Calamante, and A. Connelly, "Anatomically-constrained tractography: Improved diffusion MRI streamlines tractography through effective use of anatomical information," *NeuroImage*, vol. 62, no. 3, pp. 1924–1938, Sep. 2012.

[52] R. E. Smith, J.-D. Tournier, F. Calamante, and A. Connelly, "SIFT: Spherical-deconvolution informed filtering of tractograms," *NeuroImage*, vol. 67, pp. 298–312, Feb. 2013.

[53] J. Andersson, S. Smith, and M. Jenkinson, "NIRT-FMRIB's non-linear image registration tool," in *Proc. 14th Annu. Meeting Org. Hum. Brain Mapping*, 2008.

[54] C.-H. Yeh, R. E. Smith, T. Dhollander, F. Calamante, and A. Connelly, "Connectomes from streamlines tractography: Assigning streamlines to brain parcellations is not trivial but highly consequential," *NeuroImage*, vol. 199, pp. 160–171, Oct. 2019.

[55] H. Cheng, Y. Wang, J. Sheng, W. G. Kronenberger, V. P. Mathews, T. A. Hummer, and A. J. Saykin, "Characteristics and variability of structural networks derived from diffusion tensor imaging," *NeuroImage*, vol. 61, no. 4, pp. 64–1153, 2012.

[56] S. I. Dimitriadis, M. Drakesmith, S. Bells, G. D. Parker, D. E. Linden, and D. K. Jones, "Improving the reliability of network metrics in structural brain networks by integrating different network weighting strategies into a single graph," *Frontiers Neurosci.*, vol. 11, p. 694, Dec. 2017.

[57] A. Ghosh, Y. Rho, A. R. McIntosh, R. Kötter, and V. K. Jirsa, "Noise during rest enables the exploration of the brain's dynamic repertoire," *PLoS Comput. Biol.*, vol. 4, no. 10, Oct. 2008, Art. no. e1000196.

[58] M. Corbetta and G. L. Shulman, "Control of goal-directed and stimulus-driven attention in the brain," *Nature Rev. Neurosci.*, vol. 3, no. 3, pp. 201–215, Mar. 2002.

[59] M. D. Greicius, B. Krasnow, A. L. Reiss, and V. Menon, "Functional connectivity in the resting brain: A network analysis of the default mode hypothesis," *Proc. Nat. Acad. Sci. USA*, vol. 100, no. 1, pp. 253–258, Jan. 2003.

[60] M. D. Fox, A. Z. Snyder, J. L. Vincent, M. Corbetta, D. C. Van Essen, and M. E. Raichle, "The human brain is intrinsically organized into dynamic, anticorrelated functional networks," *Proc. Nat. Acad. Sci. USA*, vol. 102, no. 27, pp. 9673–9678, Jul. 2005.

[61] M. E. Raichle and A. Z. Snyder, "A default mode of brain function: A brief history of an evolving idea," *NeuroImage*, vol. 37, no. 4, pp. 1083–1090, Oct. 2007.

[62] M. De Luca, S. Smith, N. De Stefano, A. Federico, and P. M. Matthews, "Blood oxygenation level dependent contrast resting state networks are relevant to functional activity in the neocortical sensorimotor system," *Exp. Brain Res.*, vol. 167, no. 4, pp. 587–594, Dec. 2005.

[63] M. D. Fox, M. Corbetta, A. Z. Snyder, J. L. Vincent, and M. E. Raichle, "Spontaneous neuronal activity distinguishes human dorsal and ventral attention systems," *Proc. Nat. Acad. Sci. USA*, vol. 103, no. 26, pp. 10046–10051, Jun. 2006.

[64] J. Himberg, A. Hyvärinen, and F. Esposito, "Validating the independent components of neuroimaging time series via clustering and visualization," *NeuroImage*, vol. 22, no. 3, pp. 1214–1222, Jul. 2004.

[65] A. Abou Elseoud, T. Starck, J. Remes, J. Nikkinen, O. Tervonen, and V. Kiviniemi, "The effect of model order selection in group PICA," *Human Brain Mapping*, vol. 31, pp. 16–1207, Aug. 2009.

[66] U. Hasson, H. C. Nusbaum, and S. L. Small, "Task-dependent organization of brain regions active during rest," *Proc. Nat. Acad. Sci. USA*, vol. 106, no. 26, pp. 10841–10846, Jun. 2009.

[67] J. S. Damoiseaux, S. A. R. B. Rombouts, F. Barkhof, P. Scheltens, C. J. Stam, S. M. Smith, and C. F. Beckmann, "Consistent resting-state networks across healthy subjects," *Proc. Nat. Acad. Sci. USA*, vol. 103, no. 37, pp. 13848–13853, Sep. 2006.

[68] M. De Luca, C. F. Beckmann, N. De Stefano, P. M. Matthews, and S. M. Smith, "FMRI resting state networks define distinct modes of long-distance interactions in the human brain," *NeuroImage*, vol. 29, no. 4, pp. 1359–1367, Feb. 2006.

[69] S. M. Smith, P. T. Fox, K. L. Miller, D. C. Glahn, P. M. Fox, C. E. Mackay, N. Filippini, K. E. Watkins, R. Toro, A. R. Laird, and C. F. Beckmann, "Correspondence of the brain's functional architecture during activation and rest," *Proc. Nat. Acad. Sci. USA*, vol. 106, no. 31, pp. 13040–13045, Aug. 2009.

[70] N. B. Albert, E. M. Robertson, and R. C. Miall, "The resting human brain and motor learning," *Current Biol.*, vol. 19, no. 12, pp. 1023–1027, Jun. 2009.

[71] D. Cordes, V. M. Haughton, K. Arfanakis, G. J. Wendt, P. A. Turski, C. H. Moritz, M. A. Quigley, and M. E. Meyerand, "Mapping functionally related regions of brain with functional connectivity MR imaging," *Amer. J. Neuroradiology*, vol. 21, no. 9, pp. 1636–1644, 2000.

[72] V. Kiviniemi, J.-H. Kantola, J. Jauhiainen, A. Hyvärinen, and O. Tervonen, "Independent component analysis of nondeterministic fMRI signal sources," *NeuroImage*, vol. 19, no. 2, pp. 253–260, Jun. 2003.

[73] N. F. Dronkers, D. P. Wilkins, R. D. Van Valin, B. B. Redfern, and J. J. Jaeger, "Lesion analysis of the brain areas involved in language comprehension," *Cognition*, vol. 92, nos. 1–2, pp. 145–177, May 2004.

[74] L. Gambetti, "Evolving macroeconomic dynamics and structural change: Applications and policy implications," Ph.D. thesis, Departament d'Economia i Empresa, Universitat Pompeu Fabra, Spain, 2006.

[75] R. C. Sotero, A. Bortel, R. Martínez-Cancino, S. Neupane, P. O'Connor, F. Carbonell, and A. Shmuel, "Anatomically-constrained effective connectivity among layers in a cortical column modeled and estimated from local field potentials," *J. Integrative Neurosci.*, vol. 9, no. 4, pp. 79–355, 2010.

[76] J. M. Joyce, "Kullback–Leibler divergence," in *International Encyclopedia of Statistical Science*. Cham, Switzerland: Springer, 2011, pp. 720–722.

[77] J. Hoey, "The two-way likelihood ratio (G) test and comparison to two-way chi squared test," 2012, *arXiv:1206.4881*.

[78] E. A. Allen, E. Damaraju, S. M. Plis, E. B. Erhardt, T. Eichele, and V. D. Calhoun, "Tracking whole-brain connectivity dynamics in the resting state," *Cereb Cortex*, vol. 24, no. 3, pp. 76–663, 2014.

[79] N. Leonardi, J. Richiardi, M. Gschwind, S. Simioni, J.-M. Annoni, M. Schluep, P. Vuilleumier, and D. Van De Ville, "Principal components of functional connectivity: A new approach to study dynamic brain connectivity during rest," *NeuroImage*, vol. 83, pp. 937–950, Dec. 2013.

[80] C. Chang and G. H. Glover, "Time–frequency dynamics of resting-state brain connectivity measured with fMRI," *NeuroImage*, vol. 50, no. 1, pp. 81–98, Mar. 2010.

[81] H. Bakhshayesh, S. P. Fitzgibbon, A. S. Janani, T. S. Grummett, and K. J. Pope, "Detecting connectivity in EEG: A comparative study of data-driven effective connectivity measures," *Comput. Biol. Med.*, vol. 111, Aug. 2019, Art. no. 103329.

[82] K. Friston, L. Harrison, J. Daunizeau, S. Kiebel, C. Phillips, N. Trujillo-Barreto, R. Henson, G. Flandin, and J. Mattout, "Multiple sparse priors for the M/EEG inverse problem," *NeuroImage*, vol. 39, no. 3, pp. 1104–1120, Feb. 2008.

[83] F. von Wegner, E. Tagliazucchi, and H. Laufs, "Information-theoretical analysis of resting state EEG microstate sequences–non-markovianity, non-stationarity and periodicities," *NeuroImage*, vol. 158, pp. 99–111, Sep. 2017.

[84] K. R. Godfrey and J. J. DiStefano, "Identifiability of model parameter," *IFAC Proc. Volumes*, vol. 18, no. 5, pp. 89–114, Jul. 1985.

[85] A. Crimi, L. Dodero, F. Sambataro, V. Murino, and D. Sona, "Structurally constrained effective brain connectivity," *NeuroImage*, vol. 239, Oct. 2021, Art. no. 118288.

[86] H. Akaike, "A new look at the statistical model identification," *IEEE Trans. Autom. Control*, vol. AC-19, no. 6, pp. 716–723, Dec. 1974.

[87] S. Berman, S. Filo, and A. A. Mezer, "Modeling conduction delays in the corpus callosum using MRI-measured g-ratio," *NeuroImage*, vol. 195, pp. 128–139, Jul. 2019.

HERNAN HERNANDEZ LARZABAL received the Graduate degree from Centro Universitario José Antonio Echeverría, La Habana, Cuba. He is currently pursuing the Ph.D. degree with Universidad de Concepción, Chile. He is also a telecommunications and electronics engineer. His research interests include the study of functional signals of the human brain, diffusion magnetic resonance image processing, and machine learning.

DAVID ARAYA received the B.Sc. and P.E. degrees in electrical engineering from Universidad de Chile, Santiago, Chile, in 2005. He is currently pursuing the Ph.D. degree in biophysics and computational biology with Universidad de Valparaíso, Valparaíso, Chile. His research interests include the generative modeling of brain function, dynamic functional connectivity, active inference, and machine learning.

LAZARA LISET GONZALEZ RODRIGUEZ received the Graduate degree in telecommunications and electronics engineering from Universidad de Pinar del Río, Cuba. She is currently pursuing the Ph.D. degree with Universidad de Concepción, Chile. Her research interests include the study of diffusion magnetic resonance image processing and machine learning.

CLAUDIO ROMAN received the M.Sc. and Ph.D. degrees in electrical engineering from Universidad de Concepción, Chile. He is currently a biomedical engineer. He is also developing postdoctoral research at Universidad de Valparaîso, Chile, related to the analysis of multimodal data for studying cognitive impairment in leukemia survivors. His research interests include diffusion magnetic resonance image processing, the study of superficial white matter, and brain connectivity.

NELSON TRUJILLO-BARRETO received the B.Sc. degree (Hons.) in nuclear physics from the Higher Institute for Nuclear Science and Technology, in 1995, and the Ph.D. degree in physical sciences from Havana University, Cuba, in 2006. From 1995 to 2014, he was with the Cuban Neuroscience Centre, where he was also the Head of the Department for Brain Dynamics. Currently, he is an EPSRC Research Fellow with the Division of Neuroscience and Experimental Psychology, School of Biological Sciences, The University of Manchester, U.K.

PAMELA GUEVARA (Senior Member, IEEE) received the degree in electronics engineering from Universidad de Concepción and the master's and Ph.D. degrees in medical image analysis from Université Paris-Sud, France. She is currently a Professor with the Department of Electrical Engineering, Faculty of Engineering, Universidad de Concepción, Chile. Her research interests include the study of brain connectivity and machine learning applications, with a special focus on developing methods for analyzing dMRI tractography data. Her research is supported by ANID Chile, the Advanced Center for Electrical and Electronic Engineering (AC3E), and the National Center for Artificial Intelligence (CENIA), Chile.

WAEL EL-DEREDY received the B.Sc. degree in electrical and electronics engineering from Ain Shams University, Cairo, Egypt, the M.Sc. degree in electrical and electronics engineering from the Imperial College London, London, U.K., and the Ph.D. degree in neurocomputing from University College London, London. He is currently a Professor in computational neuroscience with Universidad de Valparaiso, Chile. His research interests include the probabilistic models of brain function, the development of novel methods for neuroimaging and application for neuroengineering, and neuroprostatics. His research is supported by MRC and EPSRC in the U.K., ANID Chile, the Advanced Center for Electrical and Electronic Engineering, Chile, and ValgrAI: The Valencian Graduate School and Research Network of Artificial Intelligence, Spain.